

SMART CAPABILITIES OF A LAMINATED PIEZOELECTRIC PLATE MODEL

L. COSTA, I. FIGUEIREDO, R. LEAL, P. OLIVEIRA AND G. STADLER

ABSTRACT: This paper focuses on the modelling and analysis of actuator and sensor effects for thin laminated plates, which are formed by stacking several layers of different piezoelectric materials. We first discuss features and properties of a two-dimensional asymptotic model for a piezoelectric anisotropic plate, whose unknowns are the Kirchhoff-Love displacement and the electric potential. We prove that the latter is a quadratic polynomial of the plate's thickness. The polynomial's coefficients depend on the tangential and transverse displacements of the plate's middle plane and the material coefficients. The asymptotic laminated plate model is discretized using finite elements. To investigate its smart capabilities we use two discrete optimization problems: the first one, focusing on the actuator effect, aims at obtaining a maximum displacement of the plate's middle plane; the second one that corresponds to the sensor effect intends to maximize the electric potential at a predefined thickness of the plate. The optimization variables are the thicknesses of the layers, their ordering as well as the location of the applied electric potential (for the actuator problem) or the location of the applied mechanical forces (for the sensor problem). Since we also want to minimize the number of these locations (besides maximizing the above objectives), we obtain a multi-objective optimization problem that we solve using genetic algorithms. Several numerical results are reported.

KEYWORDS: piezoelectric material; laminated plate; finite elements; genetic algorithms.

1. Introduction

Piezoelectric materials belong to a class of smart materials that exhibit electromechanical coupling, which provides them with actuator and sensor capabilities. The actuator effect consists in the mechanical deformation generated by the application of an external electric field to the material and the sensor effect is the converse phenomenon (cf. [1, 2]). This paper aims to analyze these effects for a thin laminated plate formed by stacking several layers of different piezoelectric anisotropic materials.

Received May 19, 2006.

This work is partially supported by the project *Mathematical analysis of piezoelectric problems* (FCT-POCI/MAT/59502/2004 of Portugal), and is part of the project *New materials, adaptive systems and their nonlinearities; modelling, control and numerical simulation* (European Community program HRN-CT-2002-00284).

We first establish, in sections 2 and 3, the two-dimensional (2D) asymptotic model for the thin laminated plate (cf. also [3] and [4, 5, 6, 7, 8] for works reporting asymptotic models for elastic and piezoelectric plates, respectively, and [9, 10, 11, 12] for the modelling and numerical simulation of piezoelectric shells). This is accomplished in two steps. Firstly, in section 2 it is proven that the asymptotic model derived in [8] (for a single thin piezoelectric plate with monoclinic elastic coefficients and modified piezoelectric coefficients independent of the plate's thickness) can be generalized to a single thin piezoelectric completely anisotropic plate (cf. theorems 2.1, 2.2 and corollary 2.1). Moreover, it is found that the solution of this 2D asymptotic model defined by (13)-(19) is the pair consisting of the Kirchhoff-Love mechanical displacement (whose tangential and transverse components are coupled in the model) and the electric potential of the plate; the latter is an explicit function of the difference of the prescribed electric potential applied on the lower and upper faces of the plate, and of the tangential and transverse displacements of the plate's middle plane (cf. (13) in theorem 2.2). In section 3, this 2D asymptotic model (13)-(19) is applied to a thin laminated plate formed by stacking several layers of different piezoelectric anisotropic materials. Assuming the material coefficients of each layer are independent of the layer's thickness, we prove that the electric potential is a quadratic polynomial of the plate's thickness (cf. (33)).

In section 4, the finite element model corresponding to the 2D asymptotic laminated plate model derived in section 3 is defined. It consists of a linear system, whose solution is the vector of tangential and transverse displacements of the plate's middle plane, and a discrete formula for the electric potential (cf. theorem 4.1 and formulas (37) and (40)). The matrix of this linear system is non-symmetric, and the right-hand side is a vector that depends on the applied mechanical forces and the difference of the electric potential applied on the lower and upper face of the plate.

Section 5 describes the numerical formulation and procedure for the analysis of the actuator as well as sensor capabilities of the discrete 2D asymptotic laminated plate introduced in section 4 (cf. also [13, 14, 15] for the analysis, modelling and numerical simulation of piezoelectric actuators). The actuator and sensor problems are defined separately, and both are formulated as multi-objective optimization problems (with non-differentiable objective functionals), which are solved by the elitist genetic algorithms described in

[16]. We observe that the actuator problem considered in this section constitutes a continuation and generalization of a previous work (cf. [17]), namely to laminated piezoelectric plates. In [17] we have applied genetic algorithms to analyze the actuator effect of a single piezoelectric and monoclinic plate. In this simpler asymptotic model defined in [8] the tangential and transverse mechanical displacements are uncoupled.

Finally several numerical tests are reported in section 6. These illustrate the actuator and the sensor capabilities of a thin laminated plate formed by two piezoelectric anisotropic layers (made of PZT materials).

2. The asymptotic model

In this section we first describe some notations and recall the three-dimensional (3D) equations for a single thin piezoelectric anisotropic plate. Then, we briefly sketch in theorem 2.1 the variational formulation of the corresponding two-dimensional (2D) asymptotic model. Moreover, we prove in theorem 2.2 that this variational formulation is equivalent to a more simple one, and finally, we observe in corollary 2.1 that this theorem 2.2 generalizes theorem 3.4 of [8].

2.1. The 3D piezoelectric plate model. Let $OX_1X_2X_3$ be a fixed three-dimensional coordinate system, $\omega \subset \mathbb{R}^2$ a bounded domain with a Lipschitz continuous boundary $\partial\omega$, and $\gamma_0, \gamma_1, \gamma_e$ and γ_s subsets of $\partial\omega$, such that, $\gamma_0 \neq \emptyset$, $\gamma_1 = \partial\omega \setminus \gamma_0$, $\emptyset \subseteq \gamma_e$, and $\gamma_s = \partial\omega \setminus \gamma_e$. We consider the sets

$$\begin{aligned} \Omega &= \omega \times (-h, h), & \Gamma_{\pm} &= \omega \times \{\pm h\}, & \Gamma_+ &= \omega \times \{+h\}, & \Gamma_- &= \omega \times \{-h\}, \\ \Gamma_D &= \gamma_0 \times (-h, h), & \Gamma_1 &= \gamma_1 \times (-h, h), & \Gamma_N &= \Gamma_1 \cup \Gamma_{\pm}, \\ \Gamma_{eN} &= \gamma_s \times (-h, h), & \Gamma_{eD} &= \Gamma_{\pm} \cup (\gamma_e \times (-h, h)), \end{aligned}$$

where $\bar{\Omega} = \bar{\omega} \times [-h, h]$ (that is, Ω and its boundary) represents a thin plate with middle surface ω and thickness $2h$, with $h > 0$ a small constant, Γ_+ and Γ_- are, respectively, the upper and lower faces of Ω , the sets Γ_D, Γ_1 and Γ_{eN} are portions of the lateral surface $\partial\omega \times (-h, h)$ of Ω , and finally Γ_N and Γ_{eD} are portions of the boundary $\partial\Omega$ of Ω . The points of Ω are denoted by $x = (x_1, x_2, x_3)$, where the first two components $(x_1, x_2) \in \omega$ and $x_3 \in (-h, h)$.

Throughout the paper, the Latin indices $i, j, k, l \dots$ belong to the set $\{1, 2, 3\}$, the Greek indices $\alpha, \beta, \mu \dots$ vary in the set $\{1, 2\}$ and the summation convention with respect to repeated indices is employed, that is,

$a_i b_i = \sum_{i=1}^3 a_i b_i$. Moreover, we denote by $a \cdot b = a_i b_i$ the inner product of the vectors $a = (a_i)$ and $b = (b_i)$. The upper subscript \top represents the transpose of a matrix or a vector. Given a function $\theta(x)$ defined in Ω we denote by $\theta_{,i}$ or $\partial_i \theta$ its partial derivative with respect to x_i , that is, $\theta_{,i} = \partial_i \theta = \frac{\partial \theta}{\partial x_i}$, and by $\theta_{,ij}$ or $\partial_{ij} \theta$ its second partial derivative with respect to x_i and x_j , that is, $\theta_{,ij} = \partial_{ij} \theta = \frac{\partial^2 \theta}{\partial x_i \partial x_j}$. We denote by $\nu = (\nu_1, \nu_2, \nu_3)$ the outward unit normal vector to $\partial\Omega$, by the same letter $\nu = (\nu_1, \nu_2)$ the outward unit normal vector to $\partial\omega$, and finally by $\partial_\nu \vartheta = \nu_\alpha \partial_\alpha \vartheta$ the outer normal derivative along $\partial\omega$ of $\vartheta : \omega \rightarrow \mathbb{R}$.

Now, let Ξ represent any open subset of \mathbb{R}^n , with $n = 2, 3$. We define $\mathcal{D}(\Xi)$ to be the linear space of functions infinitely differentiable and with compact support on Ξ , and denote by $\mathcal{D}'(\Xi)$ the dual space of $\mathcal{D}(\Xi)$, often called the space of distributions on Ξ . For $m = 1$ or $m = 2$ and $p = 2$, the Sobolev spaces $H^m(\Xi)$ (also denoted by $W^{m,2}(\Xi)$) are defined by

$$\begin{aligned} H^1(\Xi) &= \{v \in L^2(\Xi) : \partial_i v \in L^2(\Xi), \quad \text{for } i = 1, \dots, n\}, \\ H^2(\Xi) &= \{v \in L^2(\Xi) : \partial_i v, \partial_{ij} v \in L^2(\Xi), \quad \text{for } i, j = 1, \dots, n\}, \end{aligned}$$

where $L^2(\Xi) = \{v : \Xi \rightarrow \mathbb{R}, \int_\Xi |v|^2 d\Xi < +\infty\}$ and the partial derivatives are interpreted as distributional derivatives.

We suppose that a single piezoelectric anisotropic and nonhomogeneous material occupies the bounded thin plate $\bar{\Omega} \subset \mathbb{R}^3$. We denote by $C = (C_{ijkl})$, $P = (P_{ijk})$ and $\varepsilon = (\varepsilon_{ij})$, respectively, the elastic (fourth-order) tensor field, the piezoelectric (third-order) tensor field, and the dielectric (second-order) tensor field that characterize the material properties. The coefficients C_{ijkl} , P_{ijk} , ε_{ij} are sufficiently smooth functions defined in $\bar{\omega} \times [-h, h]$ that satisfy the following symmetry properties: $P_{ijk} = P_{ikj}$, $\varepsilon_{ij} = \varepsilon_{ji}$, $C_{ijkl} = C_{jikl} = C_{klij}$.

Moreover, the plate is clamped along Γ_D , and subject to an applied electric potential φ_0 on Γ_{eD} (φ_0^+ and φ_0^- are the restrictions of φ_0 to Γ_+ and Γ_- , respectively). In addition, $f = (f_i) : \Omega \rightarrow \mathbb{R}^3$ represents the density of the applied body forces acting on the plate $\bar{\Omega}$, $g = (g_i) : \Gamma_N \rightarrow \mathbb{R}^3$ the density of the applied surface forces on Γ_N (g^+ and g^- are the restriction of g to Γ_+ and Γ_- , respectively). We assume that there is neither electric charge in Ω (this means that the material is dielectric) nor on Γ_{eN} .

In the framework of small deformations and linear piezoelectricity, the three-dimensional static equations for the piezoelectric plate are the following: *Find a displacement vector field $u : \Omega \rightarrow \mathbb{R}^3$ and an electric potential*

$\varphi : \Omega \rightarrow \mathbb{R}^3$ such that

$$\sigma_{ij} = C_{ijkl}e_{kl}(u) - P_{kij}E_k(\varphi), \quad \text{in } \Omega, \quad (1)$$

$$D_k = P_{kij}e_{ij}(u) + \varepsilon_{kl}E_l(\varphi), \quad \text{in } \Omega, \quad (2)$$

$$\sigma_{ij,j} = -f_i, \quad \text{in } \Omega, \quad (3)$$

$$D_{i,i} = 0, \quad \text{in } \Omega, \quad (4)$$

$$u = 0, \quad \text{on } \Gamma_D, \quad \sigma_{ij}\nu_j = g_i, \quad \text{on } \Gamma_N, \quad (5)$$

$$D_i\nu_i = 0, \quad \text{on } \Gamma_{eN}, \quad \varphi = \varphi_0, \quad \text{on } \Gamma_{eD}. \quad (6)$$

In (1-6), $\sigma = (\sigma_{ij}) : \Omega \rightarrow \mathbb{R}^9$ is the stress tensor field, $D = (D_k) : \Omega \rightarrow \mathbb{R}^3$ the electric displacement vector field. and $e(u)$ the linear strain tensor defined by

$$e(u) = (e_{ij}(u)), \quad e_{ij}(u) = \frac{1}{2}(\partial_i u_j + \partial_j u_i),$$

and $E(\varphi)$ is the electric vector field defined by

$$E(\varphi) = (E_i(\varphi)), \quad E_i(\varphi) = -\partial_i \varphi.$$

The equations (1-2) are the constitutive equations evidencing the electromechanical coupling, (3) represents the equilibrium mechanical equation, (4) the Maxwell-Gauss equation, (5) are the displacement and traction boundary conditions, and finally (6) represents the electric boundary conditions.

2.2. The 2D asymptotic piezoelectric anisotropic plate model. Now, we apply the asymptotic analysis procedure to the variational formulation of the 3D piezoelectric anisotropic plate model (1)-(6). As the plate thickness $2h$ approaches 0, this 3D model leads to a reduced 2D model. The variational formulation of this reduced model, henceforth called the 2D asymptotic piezoelectric anisotropic plate model (or shortly, the 2D asymptotic plate model) is described in the next theorem.

In the sequel, let V_{KL} be the Kirchhoff-Love mechanical displacement space defined by

$$V_{KL} = \left\{ v = (v_1, v_2, v_3) \in [H^1(\Omega)]^3 : \begin{aligned} &\exists \eta = (\eta_1, \eta_2, \eta_3) \in [H^1(\omega)]^2 \times H^2(\omega), \\ &v_\alpha(x) = \eta_\alpha(x_1, x_2) - x_3 \partial_\alpha \eta_3(x_1, x_2), \quad v_3(x) = \eta_3(x_1, x_2), \\ &\eta_{1|\gamma_0} = \eta_{2|\gamma_0} = \eta_{3|\gamma_0} = 0, \quad \partial_\nu \eta_{3|\gamma_0} = 0 \end{aligned} \right\}$$

and Ψ_l, Ψ_{l_0} the spaces associated to the admissible electric potentials defined by

$$\begin{aligned}\Psi_l &= \{\psi \in L^2(\Omega) : \partial_3 \psi \in L^2(\Omega)\}, \\ \Psi_{l_0} &= \{\psi \in L^2(\Omega) : \partial_3 \psi \in L^2(\Omega), \psi|_{\Gamma_{\pm}} = 0\}.\end{aligned}$$

Theorem 2.1. *The variational formulation of the 2D asymptotic piezoelectric anisotropic plate model is*

$$\begin{cases} \text{Find } (u, \varphi) \in V_{KL} \times \Psi_l \text{ such that:} \\ a((u, \varphi), (v, \psi)) = l(v, \psi), \quad \forall (v, \psi) \in V_{KL} \times \Psi_{l_0}, \\ \varphi = \varphi_0, \quad \text{on } \Gamma_{\pm}, \end{cases} \quad (7)$$

where

$$\begin{cases} a((u, \varphi), (v, \psi)) = \int_{\Omega} A_{\alpha\beta\gamma\rho} e_{\alpha\beta}(u) e_{\gamma\rho}(v) d\Omega + \int_{\Omega} p_{33} \partial_3 \varphi \partial_3 \psi d\Omega \\ - \int_{\Omega} p_{3\alpha\beta} [e_{\alpha\beta}(u) \partial_3 \psi - e_{\alpha\beta}(v) \partial_3 \varphi] d\Omega, \end{cases} \quad (8)$$

and

$$l(v, \psi) = \int_{\Omega} f \cdot v d\Omega + \int_{\Gamma_N} g \cdot v d\Gamma_N, \quad (9)$$

with $A_{\alpha\beta\gamma\rho}$, $p_{3\alpha\beta}$ and p_{33} being the modified coefficients depending only on C_{ijkl} , P_{ijk} and ε_{ij} .

Proof – The proof is a trivial extension, of theorem 3.3 in [8] (established for the case $C_{\alpha\beta\gamma 3} = 0 = C_{\alpha 333}$) to the general case of anisotropy.

We recall that for the case $C_{\alpha\beta\gamma 3} = 0 = C_{\alpha 333}$, the so-called reduced elastic coefficients $A_{\alpha\beta\gamma\rho}$ are defined by (cf. formula (41) in [8])

$$A_{\alpha\beta\gamma\rho} = C_{\alpha\beta\gamma\rho} - \frac{C_{\alpha\beta 33} C_{33\gamma\rho}}{C_{3333}}, \quad (10)$$

the modified piezoelectric coefficients $p_{3\alpha\beta}$ and corresponding vector p_3 are equal to (cf. formula (42) in [8])

$$p_{3\alpha\beta} = P_{3\alpha\beta} - \frac{C_{\alpha\beta 33}}{C_{3333}} P_{333}, \quad p_3 = [p_{311} \ p_{322} \ p_{312}], \quad (11)$$

and the scalar field p_{33} is (cf. formula (43) in [8])

$$\left\{ \begin{array}{l} p_{33} = \varepsilon_{33} + \frac{P_{333}P_{333}}{C_{3333}} \\ + \frac{1}{\det \begin{bmatrix} C_{1313} & C_{1323} \\ C_{2313} & C_{2323} \end{bmatrix}} \begin{bmatrix} P_{323} \\ -P_{313} \end{bmatrix}^\top \begin{bmatrix} C_{1313} & C_{1323} \\ C_{2313} & C_{2323} \end{bmatrix} \begin{bmatrix} P_{323} \\ -P_{313} \end{bmatrix} \end{array} \right. \quad (12)$$

For the general case of anisotropy, where there are 21 independent elastic coefficients C_{ijkl} , the modified coefficients $A_{\alpha\beta\gamma\rho}$, $p_{3\alpha\beta}$ and p_{33} are defined by the terms indicated on the right-hand sides of (10), (11) and (12), respectively, plus terms containing the nonzero elastic coefficients $C_{\alpha\beta\gamma 3}$ and $C_{\alpha 333}$ that multiply some of the coefficients C_{ijkl} and/or P_{ijk} (see appendix). The procedure to obtain these formulas for $A_{\alpha\beta\gamma\rho}$, $p_{3\alpha\beta}$ and p_{33} in the general case of anisotropy is the same as indicated in [8] (cf. section 5 in [8]). It suffices to use the equations (35) in [8] with nonzero $C_{\alpha\beta\gamma 3}$ and $C_{\alpha 333}$ to derive the new formulas for κ_{ij} (cf. (34) in [8]) and subsequently introduce these κ_{ij} in the two equations of formula (40) of [8]. The latter step results in the formulas for $A_{\alpha\beta\gamma\rho}$, $p_{3\alpha\beta}$ and p_{33} . ■

Remark 2.1. *In section 6 we consider a laminated plate, whose layers are made of monoclinic piezoelectric materials with elastic, piezoelectric and dielectric coefficients that are independent of the layers' thicknesses. Thus, the material of each layer satisfies $C_{\alpha\beta\gamma 3} = 0 = C_{\alpha 333}$, and therefore, for each layer the corresponding coefficients $A_{\alpha\beta\gamma\rho}$, $p_{3\alpha\beta}$ and p_{33} are defined by (10–12).*

It is also proven in [8], theorem 3.3, that for the case of a single plate with $C_{\alpha\beta\gamma 3} = 0 = C_{\alpha 333}$, problem (7) has a unique solution (u, φ) . This result is still valid for a laminated plate, whose layers are made of monoclinic piezoelectric materials as those considered in section 6.

A straightforward computation shows that (7) can be reformulated: in fact, it is equivalent to an easier model, in which the Kirchhoff-Love displacement u is the unique solution of a two-dimensional piezoelectric plate model defined on the plate's middle plane. Provided u has been found, the electric potential φ is an explicit function of the prescribed electric potential on the lower and

upper surface and the tangential and transverse components of this Kirchhoff-Love mechanical displacement u . This result is stated and proved in the next theorem 2.2.

Theorem 2.2 (Equivalent reformulation of Problem (7)). *Let $(u, \varphi) \in V_{KL} \times \Psi_l$ be the unique solution of problem (7), where $u_\alpha = \xi_\alpha - x_3 \partial_\alpha \xi_3$, $u_3 = \xi_3$, and $\xi = (\xi_1, \xi_2, \xi_3)$. Then, the electric potential φ satisfies*

$$\begin{cases} \varphi(x_1, x_2, x_3) = \varphi_0^-(x_1, x_2) + \\ \int_{-h}^{x_3} \left[\left(\frac{p_{3\alpha\beta}}{p_{33}} - \frac{a_{\alpha\beta}}{p_{33}} c \right) e_{\alpha\beta}(\xi) - \left(\frac{p_{3\alpha\beta}}{p_{33}} y_3 - \frac{b_{\alpha\beta}}{p_{33}} c \right) \partial_{\alpha\beta} \xi_3 + \frac{\varphi_0^+ - \varphi_0^-}{p_{33}} c \right] dy_3, \end{cases} \quad (13)$$

where φ_0^+ and φ_0^- are the restrictions of φ_0 to Γ_+ and Γ_- , respectively, and

$$a_{\alpha\beta} = \int_{-h}^{+h} \frac{p_{3\alpha\beta}}{p_{33}} dx_3, \quad b_{\alpha\beta} = \int_{-h}^{+h} x_3 \frac{p_{3\alpha\beta}}{p_{33}} dx_3, \quad c = \left(\int_{-h}^{+h} \frac{1}{p_{33}} dx_3 \right)^{-1} \quad (14)$$

are functions defined on the middle plane w of the plate. Moreover, $u \in V_{KL}$ is the solution of the variational equation

$$\text{Find } u \in V_{KL} \text{ such that: } \bar{a}(u, v) = \bar{l}(v) \quad \forall v \in V_{KL}, \quad (15)$$

where for any $v = (\eta_1 - x_3 \partial_1 \eta_3, \eta_2 - x_3 \partial_2 \eta_3, \eta_3) \in V_{KL}$

$$\bar{l}(v) = \int_{\Omega} f \cdot v \, d\Omega + \int_{\Gamma_N} g \cdot v \, d\Gamma_N - \int_{\Omega} (\varphi_0^+ - \varphi_0^-) \frac{p_{3\alpha\beta}}{p_{33}} c e_{\alpha\beta}(v) \, d\Omega, \quad (16)$$

and

$$\bar{a}(u, v) = \int_{\omega} \left[N_{\alpha\beta}(u) e_{\alpha\beta}(\eta) + M_{\alpha\beta}(u) \partial_{\alpha\beta} \eta_3 \right] d\omega. \quad (17)$$

Here, $(N_{\alpha\beta}(u))$ and $(M_{\alpha\beta}(u))$ are the components of second-order tensor fields associated to the Kirchhoff-Love displacement u given by the following matrix formula

$$\begin{bmatrix} N_{\alpha\beta}(u) \\ M_{\alpha\beta}(u) \end{bmatrix} = O \begin{bmatrix} e_{\gamma\rho}(\xi) \\ \partial_{\gamma\rho} \xi_3 \end{bmatrix},$$

where the 6×6 matrix O is (in general) non-symmetric. Its components are functions of the middle plane ω , namely

$$O = \begin{bmatrix} \int_{-h}^{+h} B_{\alpha\beta\gamma\rho} dx_3 & - \int_{-h}^{+h} D_{\alpha\beta\gamma\rho} dx_3 \\ - \int_{-h}^{+h} x_3 B_{\alpha\beta\gamma\rho} dx_3 & \int_{-h}^{+h} x_3 D_{\alpha\beta\gamma\rho} dx_3 \end{bmatrix}_{6 \times 6} \quad (18)$$

with

$$\begin{aligned} B_{\alpha\beta\gamma\rho} &= A_{\alpha\beta\gamma\rho} + \frac{p_{3\alpha\beta} p_{3\gamma\rho}}{p_{33}} - \frac{p_{3\alpha\beta} a_{\gamma\rho}}{p_{33}} c \\ D_{\alpha\beta\gamma\rho} &= x_3 A_{\alpha\beta\gamma\rho} + x_3 \frac{p_{3\alpha\beta} p_{3\gamma\rho}}{p_{33}} - \frac{p_{3\alpha\beta} b_{\gamma\rho}}{p_{33}} c. \end{aligned} \quad (19)$$

In particular, the bilinear form $\bar{a}(\cdot, \cdot)$ in (17) is non-symmetric (if O is non-symmetric), and the tangential (ξ_1, ξ_2) and transverse ξ_3 components of the unknown displacement u are coupled in (15).

Proof – Considering $v = 0$ in (7) we obtain

$$\int_{\Omega} \left[p_{33} \partial_3 \varphi - p_{3\alpha\beta} e_{\alpha\beta}(u) \right] \partial_3 \psi \, d\Omega = 0.$$

Since $\mathcal{D}(\Omega)$ is dense in Ψ_{10} (see, e.g., [6]), we can take $\psi \in \mathcal{D}(\Omega)$, which gives

$$- \int_{\Omega} \partial_3 \left[p_{33} \partial_3 \varphi - p_{3\alpha\beta} e_{\alpha\beta}(u) \right] \psi \, d\Omega = 0.$$

Hence, $\partial_3 [p_{33} \partial_3 \varphi - p_{3\alpha\beta} e_{\alpha\beta}(u)] = 0$ and thus, there exists $d^1 \in \mathcal{D}'(\omega)$ such that

$$-p_{33} \partial_3 \varphi + p_{3\alpha\beta} e_{\alpha\beta}(u) = d^1 \quad \text{in } \mathcal{D}'(\omega),$$

or equivalently, because $e_{\alpha\beta}(u) = e_{\alpha\beta}(\xi) - x_3 \partial_{\alpha\beta} \xi_3$,

$$\partial_3 \varphi = \frac{p_{3\alpha\beta}}{p_{33}} [e_{\alpha\beta}(\xi) - x_3 \partial_{\alpha\beta} \xi_3] - \frac{1}{p_{33}} d^1. \quad (20)$$

After integration over x_3 this yields

$$\begin{cases} \varphi(x_1, x_2, x_3) = \varphi(x_1, x_2, -h) + \\ \int_{-h}^{x_3} \frac{p_{3\alpha\beta}}{p_{33}} [e_{\alpha\beta}(\xi) - y_3 \partial_{\alpha\beta} \xi_3] \, dy_3 - \int_{-h}^{x_3} \frac{1}{p_{33}} d^1 \, dy_3. \end{cases} \quad (21)$$

Since $\varphi(x_1, x_2, -h) = \varphi_0^-(x_1, x_2)$ and $\varphi(x_1, x_2, +h) = \varphi_0^+(x_1, x_2)$ we choose $x_3 = +h$ in the previous expression to determine d^1 :

$$\begin{cases} \varphi(x_1, x_2, +h) = \varphi(x_1, x_2, -h) + \\ \left(\int_{-h}^{+h} \frac{p_{3\alpha\beta}}{p_{33}} \, dx_3 \right) e_{\alpha\beta}(\xi) - \left(\int_{-h}^{+h} x_3 \frac{p_{3\alpha\beta}}{p_{33}} \, dx_3 \right) \partial_{\alpha\beta} \xi_3 - \left(\int_{-h}^{+h} \frac{1}{p_{33}} \, dx_3 \right) d^1, \end{cases}$$

and clearly this equation is exactly the same as

$$\varphi_0^+ = \varphi_0^- + a_{\alpha\beta} e_{\alpha\beta}(\xi) - b_{\alpha\beta} \partial_{\alpha\beta} \xi_3 - c^{-1} d^1,$$

or equivalently

$$d^1 = c [\varphi_0^- - \varphi_0^+ + a_{\alpha\beta} e_{\alpha\beta}(\xi) - b_{\alpha\beta} \partial_{\alpha\beta} \xi_3]. \quad (22)$$

Finally, inserting this d^1 in (21) we directly obtain formula (13) for the electric potential.

Choosing now $\psi = 0$ in (7) we get

$$\begin{cases} \int_{\Omega} A_{\alpha\beta\gamma\rho} e_{\alpha\beta}(u) e_{\gamma\rho}(v) d\Omega + \int_{\Omega} p_{3\alpha\beta} e_{\alpha\beta}(v) \partial_3 \varphi d\Omega = \\ \int_{\Omega} f \cdot v d\Omega + \int_{\Gamma_N} g \cdot v d\Gamma_N. \end{cases} \quad (23)$$

For the derivative $\partial_3 \varphi$ given in (20) with d^1 as defined in (22) we have

$$\partial_3 \varphi = \left(\frac{p_{3\alpha\beta}}{p_{33}} - \frac{a_{\alpha\beta}}{p_{33}} c \right) e_{\alpha\beta}(\xi) - \left(\frac{p_{3\alpha\beta}}{p_{33}} x_3 - \frac{b_{\alpha\beta}}{p_{33}} c \right) \partial_{\alpha\beta} \xi_3 + \frac{\varphi_0^+ - \varphi_0^-}{p_{33}} c,$$

and introducing this latter formula in (23) we obtain

$$\begin{cases} \int_{\Omega} \left[B_{\alpha\beta\gamma\rho} e_{\alpha\beta}(\xi) - D_{\alpha\beta\gamma\rho} \partial_{\gamma\rho}(\xi_3) \right] (e_{\alpha\beta}(\eta) - x_3 \partial_{\alpha\beta} \eta_3) d\Omega = \\ \int_{\Omega} f \cdot v d\Omega + \int_{\Gamma_N} g \cdot v d\Gamma_N - \int_{\Omega} (\varphi_0^+ - \varphi_0^-) \frac{p_{3\alpha\beta}}{p_{33}} c e_{\alpha\beta}(v) d\Omega, \end{cases} \quad (24)$$

which is precisely the variational equation (15). \blacksquare

For later use we remark for the last term on the right-hand side of (24) holds

$$\int_{\Omega} (\varphi_0^+ - \varphi_0^-) \frac{p_{3\alpha\beta}}{p_{33}} c e_{\alpha\beta}(v) d\Omega = \int_{\omega} (\varphi_0^+ - \varphi_0^-) c (a_{\alpha\beta} e_{\alpha\beta}(\eta) - b_{\alpha\beta} \partial_{\alpha\beta} \eta_3) d\omega. \quad (25)$$

In the next corollary 2.1 we show that theorem 2.2 is a generalization of theorem 3.4 in [8].

Corollary 2.1 (Theorem 3.4 of [8]). *Suppose that $C_{\alpha\beta\gamma 3} = 0 = C_{\alpha 333}$ and the coefficients $p_{3\alpha\beta}$ and p_{33} are independent of x_3 . Then (13) becomes*

$$\varphi(x_1, x_2, x_3) = \varphi_0^-(x_1, x_2) + \int_{-h}^{x_3} \left[- \left(\frac{p_{3\alpha\beta}}{p_{33}} y_3 \right) \partial_{\alpha\beta} \xi_3 + \frac{\varphi_0^+ - \varphi_0^-}{2h} \right] dy_3, \quad (26)$$

which is precisely the formula (88) of [8] after integration with respect to the thickness variable. Moreover, problem (15) coincides with problem (56) of [8] (we remark that $h = 1$ in (56) of [8]), because in this case

$$\bar{l}(v) = \int_{\Omega} f \cdot v dx + \int_{\Gamma_N} g \cdot v d\Gamma_N - \int_{\Omega} \frac{\varphi_0^+ - \varphi_0^-}{2h} p_{3\alpha\beta} e_{\alpha\beta}(v) dx, \quad (27)$$

and

$$\bar{a}(u, v) = \int_{\omega} \left[N_{\alpha\beta}(u) e_{\alpha\beta}(\eta) + M_{\alpha\beta}(u) \partial_{\alpha\beta}\eta_3 \right] d\omega, \quad (28)$$

where $(N_{\alpha\beta}(u))$ and $(M_{\alpha\beta}(u))$ are defined by the following matrix formula

$$\begin{aligned} \begin{bmatrix} N_{\alpha\beta}(u) \\ M_{\alpha\beta}(u) \end{bmatrix} &= O \begin{bmatrix} e_{\gamma\rho}(\xi) \\ \partial_{\gamma\rho}\xi_3 \end{bmatrix} \\ &= \begin{bmatrix} \int_{-h}^{+h} A_{\alpha\beta\gamma\rho} dx_3 & - \int_{-h}^{+h} x_3 A_{\alpha\beta\gamma\rho} dx_3 \\ - \int_{-h}^{+h} x_3 A_{\alpha\beta\gamma\rho} dx_3 & \int_{-h}^{+h} (x_3)^2 \left(A_{\alpha\beta\gamma\rho} + \frac{p_{3\alpha\beta} p_{3\gamma\rho}}{p_{33}} \right) dx_3 \end{bmatrix} \begin{bmatrix} e_{\gamma\rho}(\xi) \\ \partial_{\gamma\rho}\xi_3 \end{bmatrix} \end{aligned} \quad (29)$$

with $A_{\alpha\beta\gamma\rho}$, $p_{3\alpha\beta}$ and p_{33} given by (10)–(12).

Proof – In fact, if $p_{3\alpha\beta}$ and p_{33} are independent of x_3 , then

$$a_{\alpha\beta} = 2h \frac{p_{3\alpha\beta}}{p_{33}}, \quad b_{\alpha\beta} = 0, \quad c = \frac{p_{33}}{2h},$$

and

$$\frac{p_{3\alpha\beta}}{p_{33}} - \frac{a_{\alpha\beta}}{p_{33}} c = \frac{p_{3\alpha\beta}}{p_{33}} - 2h \frac{p_{3\alpha\beta}}{p_{33}^2} \frac{p_{33}}{2h} = 0,$$

therefore (13) turns to (26), and (27) is obtained from (16) replacing c by $\frac{p_{33}}{2h}$. We also have

$$\frac{p_{3\alpha\beta} p_{3\gamma\rho}}{p_{33}} - \frac{p_{3\alpha\beta} a_{\gamma\rho}}{p_{33}} c = \frac{p_{3\alpha\beta} p_{3\gamma\rho}}{p_{33}} - \frac{p_{3\alpha\beta}}{p_{33}} \frac{2h p_{3\gamma\rho}}{p_{33}} \frac{p_{33}}{2h} = 0.$$

Thus, the coefficients $B_{\alpha\beta\gamma\rho}$ and $D_{\alpha\beta\gamma\rho}$ defined in (19) are equal to

$$B_{\alpha\beta\gamma\rho} = A_{\alpha\beta\gamma\rho}, \quad D_{\alpha\beta\gamma\rho} = x_3 \left(A_{\alpha\beta\gamma\rho} + \frac{p_{3\alpha\beta} p_{3\gamma\rho}}{p_{33}} \right). \quad (30)$$

Consequently the bilinear formula (17-19) turns to (28-29) with the coefficients $B_{\alpha\beta\gamma\rho}$ and $D_{\alpha\beta\gamma\rho}$ defined by (30). ■

3. The laminated piezoelectric plate model

In this section, the 2D asymptotic plate model defined in theorem 2.2 is considered for the special case of a thin laminated plate made of several stacked layers of different piezoelectric anisotropic materials. We assume that for each layer the elastic, piezoelectric and dielectric coefficients are independent of the layer's thickness. This special material structure enables

particular formulas for the functions, matrices and vectors involved in the definition of the 2D asymptotic plate model of theorem 2.2. Below, we give the detailed form for the matrix O and the electric potential φ .

3.1. The matrix O . As before, the global plate $\bar{\Omega} = \bar{w} \times [-h, h]$, has middle plane $w \subset \mathbb{R}^2$ and global thickness $2h$. The material and geometric properties of each lamina are indexed by the letter s . We assume that there are k laminas, numbered from the lower face to the upper face of the global plate $\bar{\Omega}$. We do not impose any geometrical symmetry in the distribution of these k laminas with respect to the middle plane w of the global plate. Let t_s be the thickness of lamina s and $|z_s|$ the distance from w to the middle plane of lamina s , measured along the axis OX_3 , where z_s is positive if lamina s is above w and negative if it is below. In particular, the sum of the thicknesses of the k laminas must be equal to $2h$, that is $\sum_{s=1}^k t_s = 2h$.

In this setting, the coefficients $a_{\alpha\beta}$, $b_{\alpha\beta}$ and c introduced in (14) become

$$\begin{aligned} a_{\alpha\beta} &= \int_{-h}^{+h} \frac{p_{3\alpha\beta}}{p_{33}} dx_3 = \sum_{s=1}^k \frac{p_{3\alpha\beta}^s}{p_{33}^s} t_s, & b_{\alpha\beta} &= \int_{-h}^{+h} x_3 \frac{p_{3\alpha\beta}}{p_{33}} dx_3 = \sum_{s=1}^k \frac{p_{3\alpha\beta}^s}{p_{33}^s} z_s t_s, \\ c &= \left(\int_{-h}^{+h} \frac{1}{p_{33}} dx_3 \right)^{-1} = \left(\sum_{s=1}^k \frac{t_s}{p_{33}^s} \right)^{-1}, \end{aligned} \tag{31}$$

and for the components of the matrix O in (18) we get

$$\begin{aligned} \int_{-h}^{+h} B_{\alpha\beta\gamma\rho} dx_3 &= \sum_{s=1}^k \underbrace{\left[A_{\alpha\beta\gamma\rho}^s + \frac{p_{3\alpha\beta}^s p_{3\gamma\rho}^s}{p_{33}^s} - \frac{p_{3\alpha\beta}^s a_{\gamma\rho}}{p_{33}^s} c \right]}_{B_{\alpha\beta\gamma\rho}^s} t_s, \\ \int_{-h}^{+h} x_3 B_{\alpha\beta\gamma\rho} dx_3 &= \sum_{s=1}^k \underbrace{\left[A_{\alpha\beta\gamma\rho}^s + \frac{p_{3\alpha\beta}^s p_{3\gamma\rho}^s}{p_{33}^s} - \frac{p_{3\alpha\beta}^s a_{\gamma\rho}}{p_{33}^s} c \right]}_{B_{\alpha\beta\gamma\rho}^s} t_s z_s, \\ \int_{-h}^{+h} D_{\alpha\beta\gamma\rho} dx_3 &= \sum_{s=1}^k \underbrace{\left[A_{\alpha\beta\gamma\rho}^s + \frac{p_{3\alpha\beta}^s p_{3\gamma\rho}^s}{p_{33}^s} \right]}_{D_{\alpha\beta\gamma\rho}^{1s}} t_s z_s - \sum_{s=1}^k \underbrace{\left[\frac{p_{3\alpha\beta}^s b_{\gamma\rho}}{p_{33}^s} c \right]}_{D_{\alpha\beta\gamma\rho}^{2s}} t_s, \end{aligned}$$

and

$$\int_{-h}^{+h} x_3 D_{\alpha\beta\gamma\rho} dx_3 = \sum_{s=1}^k \underbrace{\left[A_{\alpha\beta\gamma\rho}^s + \frac{p_{3\alpha\beta}^s p_{3\gamma\rho}^s}{p_{33}^s} \right]}_{D_{\alpha\beta\gamma\rho}^{1s}} \frac{1}{12} (t_s^3 + 12 t_s z_s^2) - \sum_{s=1}^k \underbrace{\left[\frac{p_{3\alpha\beta}^s b_{\gamma\rho}}{p_{33}^s} c \right]}_{D_{\alpha\beta\gamma\rho}^{2s}} t_s z_s.$$

Therefore, the matrix O as defined in (18) becomes a sum O^{lam} of (in general non-symmetric) matrices, namely

$$O^{lam} = \sum_{s=1}^k \begin{bmatrix} B_{\alpha\beta\gamma\rho}^s t_s & -D_{\alpha\beta\gamma\rho}^{1s} t_s z_s + D_{\alpha\beta\gamma\rho}^{2s} t_s \\ -B_{\alpha\beta\gamma\rho}^s t_s z_s & D_{\alpha\beta\gamma\rho}^{1s} \frac{1}{12} (t_s^3 + 12 t_s z_s^2) - D_{\alpha\beta\gamma\rho}^{2s} t_s z_s \end{bmatrix}_{6 \times 6}. \quad (32)$$

This matrix (32) induces the bilinear form $\bar{a}(\cdot, \cdot)$ in (17) for the laminated plate. Note that the third term on the right-hand side of the linear form $\bar{l}(\cdot)$ in (16) is defined by (25), where the coefficients $a_{\alpha\beta}$, $b_{\alpha\beta}$ and c are given by (31).

3.2. The electric potential φ . Let us now turn to the formula of the electric potential for the case of the laminated plate. If x_3 belongs to lamina i , with $1 \leq i \leq k$, we obtain from (13)

$$\left\{ \begin{array}{l} \varphi(x_1, x_2, x_3) = \varphi_0^-(x_1, x_2) + \\ \sum_{s=1}^{i-1} \left[\left(\frac{p_{3\alpha\beta}^s}{p_{33}^s} - \frac{a_{\alpha\beta}}{p_{33}^s} c \right) t_s e_{\alpha\beta}(\xi) - \left(t_s z_s \frac{p_{3\alpha\beta}^s}{p_{33}^s} - t_s \frac{b_{\alpha\beta}}{p_{33}^s} c \right) \partial_{\alpha\beta} \xi_3 + \frac{\varphi_0^+ - \varphi_0^-}{p_{33}^s} c t_s \right] + \\ \left(\frac{p_{3\alpha\beta}^i}{p_{33}^i} - \frac{a_{\alpha\beta}}{p_{33}^i} c \right) \left(x_3 - z_i + \frac{t_i}{2} \right) e_{\alpha\beta}(\xi) - \frac{p_{3\alpha\beta}^i}{p_{33}^i} \left(x_3^2 - \left(z_i - \frac{t_i}{2} \right)^2 \right) \frac{1}{2} \partial_{\alpha\beta} \xi_3 + \\ \frac{b_{\alpha\beta}}{p_{33}^i} c \left(x_3 - z_i + \frac{t_i}{2} \right) \partial_{\alpha\beta} \xi_3 + \frac{\varphi_0^+ - \varphi_0^-}{p_{33}^i} c \left(x_3 - z_i + \frac{t_i}{2} \right). \end{array} \right. \quad (33)$$

Of course, if x_3 belongs to lamina 1, the sum $\sum_{s=1}^{i-1} [\dots]$ on the right-hand side of (33) disappears. We also remark that φ is a quadratic polynomial of the plate's thickness.

4. The discrete laminated piezoelectric plate model

The application of the finite element method to (15) and to (13) for the particular case of a thin laminated plate (cf. section 3) leads to a discrete laminated piezoelectric plate model, see theorem 4.1.

4.1. The discrete model. In the sequel, we assume that the plate's middle plane is a rectangular domain ω that is discretized using $m = n_1 n_2$ axis-parallel rectangles ω^e , i.e., $\omega = \bigcup_{e=1}^m \omega^e$. We suppose $\omega^e = [a_1^e, b_1^e] \times [c_2^e, d_2^e]$ and denote $h_1^e = b_1^e - a_1^e$ and $h_2^e = d_2^e - c_2^e$, that is, $\{\omega^e\}$ is affine equivalent to the reference element $\hat{\omega} = [-1, +1] \times [-1, +1]$.

The rectangular Melosh finite element and the Adini finite element (cf. Ciarlet [18]) are chosen to approximate the tangential and transverse displacement fields (ξ_1, ξ_2) and $u_3 = \xi_3$ of the Kirchhoff-Love displacement u , respectively. The 8 degrees of freedom of the Melosh element are the values of (ξ_1, ξ_2) at the vertices of ω^e , and the 12 degrees of freedom characterizing the Adini element are the values of $u_3, u_{3,1}$ and $u_{3,2}$ at the vertices of ω^e . In the sequel, we also utilize the 2×8 -matrix M and the vector 12×1 -vector N^e corresponding, respectively, to the four shape functions of the Melosh finite element and the twelve shape functions associated to the Adini finite element, which are defined in $\hat{\omega}$ (cf. (26) and (27) in [17]). Moreover, let L^e and S^e be the matrices that depend on the derivatives of the shape functions of the Melosh and Adini finite elements, respectively (cf. (38) and (39) in [17]).

If n is the number of nodes in the finite element mesh, as approximation of the displacements $(\xi_1, \xi_2, \xi_3, \xi_{3,1}, \xi_{3,2})$ in ω we obtain the vector $u \in \mathbb{R}^{5n}$ defined by

$$\begin{aligned} u &= [u_{tg} \quad u_{tv}] \in \mathbb{R}^{2n+3n} \quad \text{with} \\ u_{tg} &= (u_{1j}, u_{2j})_{j=1}^n, \quad u_{tv} = (u_{3j}, u_{31j}, u_{32j})_{j=1}^n, \end{aligned} \tag{34}$$

where u_{tg} and u_{tv} are, respectively, the approximations of the tangential and transverse displacements (ξ_1, ξ_2) and $(\xi_3, \xi_{3,1}, \xi_{3,2})$. This means that u_{1j}, u_{2j} and u_{3j}, u_{31j}, u_{32j} are the approximations of ξ_1, ξ_2 and $\xi_3, \xi_{3,1}, \xi_{3,2}$, respectively, at the node j of the finite element mesh ω . Moreover, if P is an arbitrary set of indices, we denote by u_{tvP}, u_{tgP} the sub-vectors of u_{tv} and u_{tg} respectively, whose components have their indices in P .

Let also

$$\begin{aligned} F_i &= \int_{-h}^{+h} f_i dx_3 + g_i^+ + g_i^-, \quad \text{for } i = 1, 2, 3, \\ f_{tg} &= [F_1 \ F_2]^\top \quad \text{and} \quad f_{tv} = F_3 \end{aligned} \quad (35)$$

be the vectors associated to the density of mechanical forces acting on the middle plane ω of the plate, and let the vectors p_3^s , a^{lam} and b^{lam} (related to the material coefficients p_3 , $a_{\alpha\beta}$ and $b_{\alpha\beta}$ of the laminated plate, cf. (11) and (31)) be defined by

$$\begin{aligned} p_3^s &= [p_{311}^s \ p_{322}^s \ p_{312}^s] \quad \text{for each layer } s, \\ a^{lam} &= [a_{11} \ a_{22} \ a_{12}], \quad b^{lam} = [b_{11} \ b_{22} \ b_{12}]. \end{aligned} \quad (36)$$

Then we have the following theorem.

Theorem 4.1. *The finite element discret problem associated to (15) takes the following form:*

$$\begin{cases} \text{Find } u = [u_{tg} \ u_{tv}] \in \mathbb{R}^{5n} & \text{such that :} \\ u_{tgI} = 0, \quad u_{tvJ} = 0, \\ Ku = F. \end{cases} \quad (37)$$

The equations $u_{tgI} = 0$ and $u_{tvJ} = 0$ represent the discrete boundary conditions for the displacements. At the element level, the square matrix K and the vector F are defined by K^e and F^e , respectively. The 20×20 matrix K^e is in general non-symmetric and strongly depends on the laminated material coefficients

$$K^e = \frac{h_1^e h_2^e}{4} \int_{\hat{\omega}} \left(\begin{bmatrix} L^{e\top} & 0 \\ 0 & S^{e\top} \end{bmatrix}_{20 \times 6} O_{6 \times 6}^{lam} \begin{bmatrix} L^e & 0 \\ 0 & S^e \end{bmatrix}_{6 \times 20} \right) d\omega^e, \quad (38)$$

where O^{lam} is the material matrix defined in (32). The vector F^e has 20 components and is related to the mechanical forces and the applied electric potential φ_0^+ and φ_0^- . Assuming that the surface mechanical force $g = 0$ in

Γ_1 and f_α , g_α^+ , g_α^- are independent of $x_3 \in [-h, h]$ we obtain

$$F^e = \begin{bmatrix} F_{tg}^e \\ F_{tv}^e \end{bmatrix}, \quad \text{where}$$

$$F_{tg}^e = \frac{h_1^e h_2^e}{4} \int_{\hat{\omega}} \left[M^\top f_{tg} - (\varphi_0^+ - \varphi_0^-) c L^{e\top} \sum_{s=1}^k \frac{p_3^{s\top}}{p_{33}^s} t_s \right] d\hat{\omega}, \quad (39)$$

$$F_{tv}^e = \frac{h_1^e h_2^e}{4} \int_{\hat{\omega}} \left[N^{e\top} f_{tv} + (\varphi_0^+ - \varphi_0^-) c S^{e\top} \sum_{s=1}^k \frac{p_3^{s\top}}{p_{33}^s} t_s z_s \right] d\hat{\omega}.$$

It is worth noticing that the nodal displacements u_{tg} and u_{tv} in (37) are coupled (due to the definition of O^{lam} in (32)).

Furthermore, if x_3 belongs to lamina i , $1 \leq i \leq k$, the finite element approximation of the electric potential (33) in $\omega^e \times (-h, +h)$ is defined by

$$\left\{ \begin{array}{l} \varphi(x_1, x_2, x_3)|_{\omega^e \times (-h, +h)} \simeq \varphi_0^- + \\ \sum_{s=1}^{i-1} \left[\left(\frac{p_3^s}{p_{33}^s} - \frac{a^{lam}}{p_{33}^s} c \right) t_s L^e u_{tg}^e - \left(t_s z_s \frac{p_3^s}{p_{33}^s} - t_s \frac{b^{lam}}{p_{33}^s} c \right) S^e u_{tv}^e + \frac{\varphi_0^+ - \varphi_0^-}{p_{33}^s} c t_s \right] + \\ \left(\frac{p_3^i}{p_{33}^i} - \frac{a^{lam}}{p_{33}^i} c \right) \left(x_3 - z_i + \frac{t_i}{2} \right) L^e u_{tg}^e - \frac{p_3^i}{p_{33}^i} \left(x_3^2 - \left(z_i - \frac{t_i}{2} \right)^2 \right) \frac{1}{2} S^e u_{tv}^e + \\ \frac{b^{lam}}{p_{33}^i} c \left(x_3 - z_i + \frac{t_i}{2} \right) S^e u_{tv}^e + \frac{\varphi_0^+ - \varphi_0^-}{p_{33}^i} c \left(x_3 - z_i + \frac{t_i}{2} \right), \end{array} \right. \quad (40)$$

and if x_3 belongs to lamina 1, the sum $\sum_{s=1}^{i-1} [\dots]$ disappears on the right-hand side of (40).

Proof – The arguments are similar to those used in theorem 3.1 in [17], so we omit the proof. Nevertheless we remark that we have assumed that the surface mechanical force $g = 0$ in Γ_1 and f_α , g_α^+ , g_α^- are independent of $x_3 \in [-h, h]$ in order to simplify the formulas for the vector F . Otherwise the expression for F^e in (39) would have more terms. Furthermore, to obtain (40) it suffices to use (33) and apply the following standard finite element

approximations for each finite element ω^e

$$\begin{aligned} (\xi_1, \xi_2) &\simeq Mu_{tg}^e, & [e_{11}(\xi) \ e_{22}(\xi) \ 2e_{12}(\xi)] &\simeq L^e u_{tg}^e, \\ u_3 = \xi_3 &\simeq N^e u_{tv}^e, & [\partial_{11}\xi_3 \ \partial_{22}\xi_3 \ 2\partial_{12}\xi_3] &\simeq S^e u_{tv}^e. \quad \blacksquare \end{aligned}$$

Remark 4.1. - *The finite element code producing the discrete model described in the previous theorem is available on request (cf. <http://www.mat.uc.pt/~isabelf/poci59502.html>, code *Lampiezo.m*).*

5. Optimization problems

We now describe the optimization problems that model the actuator and the sensor effect of the discrete 2D laminated piezoelectric plate model (defined in theorem 4.1). For the actuator problem we vary the location of the applied electric potential difference $\varphi_0^+ - \varphi_0^-$, and for the sensor problem the location of the applied mechanical loads. Moreover, for both problems, we may also change the order of the different materials and the thickness of each lamina. Before presenting the actuator and sensor optimization problems, we define the optimization variables.

5.1. Optimization variables. There are three optimization variables: the vector t of thicknesses, the vector mat of materials and the vector loc representing the location, in the plate's middle plane ω , of the non-zero applied electric potential difference $\varphi_0^+ - \varphi_0^-$ or the non-zero applied mechanical loads f_{tg} and f_{tv} . The vectors t and mat are defined by

$$\begin{aligned} t &= (t_1, t_2, \dots, t_k), \quad \text{with} \quad \sum_{s=1}^k t_s = 2h, \quad t_s > 0, \\ mat &= (mat_1, mat_2, \dots, mat_k), \quad mat_r \neq mat_s, \quad \text{for } r = s + 1. \end{aligned} \tag{41}$$

The components of both vectors are numbered from the lower to the upper face of the laminated plate, and layers with zero thickness or repeated materials are not allowed.

Next we define the vector loc . We assume that the non-zero applied electric potential differences or mechanical loads may act in regions of ω with the same size. These regions are numbered and the finite element discretization of ω is chosen such that the borders of the regions consist of edges of adjacent finite elements. Then, the optimization variable loc is defined by

$$loc = (i, j, pe), \tag{42}$$

where $1 \leq i \leq m_j$ is the number of regions of ω that consist of $j \geq 1$ adjacent finite elements (m_j is the total number of regions), where the non-zero electric potential difference or mechanical loads are applied. The set pe contains i elements of $Y_j = \{1, 2, \dots, m_j\}$ representing the location of these regions. In particular, pe ranges over all subsets of Y_j with cardinality i , that is, $pe \in C_i^{m_j}(Y_j)$.

For example, for a rectangular mesh with 20×20 finite elements setting $loc = (3, 4 \times 4, [1, 4, 8])$ means that the non-zero applied electric potential difference or non-zero applied mechanical loads are acting in 3 regions of ω , each consisting of $4 \times 4 = 16$ finite elements, located at the positions $pe = [1, 4, 8]$ of $Y_{16} = \{1, \dots, m_{16} = 25\}$.

Since the size of the regions with nonzero electric potential difference or mechanical load is independent of the finite element mesh, for finer meshes the number of adjacent finite elements j corresponding to the regions in loc increases. Obviously, for a mesh with m finite elements, $1 \leq m_j \leq m$ holds for any j and $m_j = m$ for $j = 1$.

5.2. Actuator optimization problem. The actuator effect of a piezoelectric material (also called the inverse piezoelectric effect) is by definition the mechanical deformation generated by the application of an external electric field to the material. The aim of this subsection is to present the optimization problem that focuses on the maximization of the actuator effect of the laminated piezoelectric plate model.

For a mesh with m finite elements and n global nodes, the mechanical displacement of the plate is determined by the displacements (ξ_1, ξ_2, ξ_3) that define the Kirchhoff-Love displacement u of the nodes in the plate's middle plane. For an arbitrary node j in the middle plane's mesh, the corresponding three-dimensional displacement (ξ_1, ξ_2, ξ_3) is approximated by (u_{1j}, u_{2j}, u_{3j}) . Fixing the applied mechanical forces and the boundary conditions, the nodes' displacements depend on the location of the non-zero applied electric potential difference $loc = (i, j, pe)$ as well as on the thickness and material vector $t = (t_1, \dots, t_k)$ and $mat = (mat_1, \dots, mat_k)$. Of course, for each fixed triple (loc, t, mat) there exists a node in the mesh that attains a maximum displacement $d(loc, t, mat)$, that is

$$d(loc, t, mat) = \max_{j=1, \dots, n} \|(u_{1j}, u_{2j}, u_{3j})\|_{\mathbb{R}^3}, \quad (43)$$

where $\|\cdot\|_{\mathbb{R}^3}$ is the usual Euclidean norm in \mathbb{R}^3 .

Our objective is to maximize $d(loc, t, mat)$ choosing appropriate $loc = (i, j, pe)$, $t = (t_1, \dots, t_k)$ and $mat = (mat_1, \dots, mat_k)$, where pe ranges over all the subsets of Y_j with i distinct elements. At the same time we want to minimize the number i of regions of ω with nonzero electric potential difference. Therefore, two objectives are considered: the maximization of the displacements and the minimization of the number i of regions. This corresponds to the following actuator multi-objective optimization problem with non-differentiable functional

$$\left[\begin{array}{l} \max_{(loc, t, mat)} d(loc, t, mat) = \max_{(loc, t, mat)} \left(\overbrace{\max_{j=1, \dots, n} \|(u_{1j}, u_{2j}, u_{3j})\|_{\mathbb{R}^3}}^{d(loc, t, mat)} \right) \wedge \min i \\ \text{subject to :} \left\{ \begin{array}{l} loc = (i, j, pe), \quad pe \in C_i^{m_j}(Y_j), \quad \#pe = i, \quad i = 1, 2, \dots, m_j, \\ t = (t_1, t_2, \dots, t_k), \quad \sum_{s=1}^k t_s = 2h, \quad t_s > 0, \quad s = 1, \dots, k, \\ mat = (mat_1, mat_2, \dots, mat_k), \quad mat_r \neq mat_s, \quad \text{for } r = s + 1, \\ \left\{ \begin{array}{l} \text{Find } u = [u_{tg} \ u_{tv}] \in \mathbb{R}^{5n} \text{ such that :} \\ u_{tgI_1} = u_{tgI_2} = 0, \quad u_{tvJ_1} = u_{tvJ_2} = u_{tvJ_3} = 0, \\ Ku = F_{(loc, t, mat)}. \end{array} \right. \end{array} \right. \end{array} \right. \quad (44)$$

We observe that the vector F depends on (loc, t, mat) , cf. (39). To emphasize this dependence we write $F_{(loc, t, mat)}$ instead of F .

Note that for multi-objective problems such as (44) the aim is to characterize the set of so-called Pareto optimal solutions; these are solutions that cannot improve the performance of the first objective function (the node's displacement $d(loc, t, mat)$) without worsening the performance of the second one (the number i of regions where the applied electric potential difference is non-zero) and vice-versa. If we drop the second objective, that is $\min i$, the multi-objective problem becomes an optimization problem with only one objective, namely to achieve a maximal node's displacement choosing (loc, t, mat) appropriately for fixed i in loc .

It should be referred that (44) is a combinatorial problem, since different combinations of the positions for the applied electric potentials, of the layer's thicknesses and the order of the materials produce different node's displacements. In particular, the set $C_i^{m_j}(Y_j)$ that is the admissible set for the optimization variable pe is of cardinality $C_i^{m_j} = \frac{m_j!}{i!(m_j-i)!}$ (for instance, for

a mesh with $m_j = 25$ and $i = 3$ we have $C_3^{25} = 2300$). However, the number $C_i^{m_j}$ can be reduced if the problem has some symmetry.

Obviously, the solutions of the optimization problem (44) strongly depend on the mechanical loadings and the boundary conditions imposed to the plate. In order to achieve a better understanding of the actuator effect, we assume that all the mechanical loadings $f = (f_i)$ and $g = (g_i)$ vanish. To analyze the influence of the boundary conditions, we consider the plate to be clamped on different parts of the lateral surface (this means that we vary the definition of the set $\gamma_0 \subset \partial\omega$).

5.3. Sensor optimization problem. The sensor effect of a piezoelectric material (also called the direct piezoelectric effect) consists in the generation of an electric field in the material that is subject to an imposed mechanical force. In this subsection we describe the optimization problem related to the maximization of the sensor effect of the discrete laminated piezoelectric plate model. The optimization variables are those defined above, that is, (loc, t, mat) . As objective functional we choose the maximum value of the electric potential φ (cf. (40)) at a pre-defined thickness z_s for each lamina s , that is, for a mesh with m finite elements we consider the non-differentiable function

$$elpot(loc, t, mat) = \max_{e=1, \dots, m} \max_{s=1, \dots, k} |\varphi|_{\omega^e \times \{z_s\}}|. \quad (45)$$

We notice that the discrete electric potential $\varphi|_{\omega^e \times (-h, +h)}$ depends on (loc, t, mat) by means of the Kirchhoff-Love displacement u , which is the solution of $Ku = F_{(loc, t, mat)}$, cf. (37) and (40).

Analogously to the actuator optimization problem the objective is not only to maximize $elpot(loc, t, mat)$, but also to minimize the number i of regions of ω with non-zero mechanical forces. Therefore, two objectives are considered,

which leads to the following sensor multi-objective optimization problem

$$\left[\begin{array}{l} \max_{(loc,t,mat)} elpot(loc,t,mat) = \max_{(loc,t,mat)} \left(\overbrace{\max_{e=1,\dots,m} \max_{s=1,\dots,k} |\varphi|_{\omega^e \times \{z_s\}}}^{elpot(loc,t,mat)} \right) \wedge \min i \\ \text{subject to :} \left[\begin{array}{l} loc = (i,j,pe), \quad pe \in C_i^{m_j}(Y_j), \quad \#pe = i, \quad i = 1, 2, \dots, m_j, \\ t = (t_1, t_2, \dots, t_k), \quad \sum_{s=1}^k t_s = 2h, \quad t_s > 0, \quad s = 1, \dots, k, \\ mat = (mat_1, mat_2, \dots, mat_k), \quad mat_r \neq mat_s, \quad \text{if } r = s + 1, \\ \varphi|_{\omega^e \times \{z_s\}} \quad \text{defined in (40)}. \end{array} \right. \end{array} \right. \quad (46)$$

Unlike the actuator optimization problem we assume in this case non zero mechanical forces and applied electric potential all nil.

6. Numerical tests

In this section, we describe the data and the solutions of our numerical tests. Moreover, we give a brief explanation of the genetic algorithms used to solve the multi-objective optimization problems (44) and (46).

6.1. Data. Let us now consider a fixed three-dimensional coordinate system $OXYZ$ and a laminated plate $\bar{\Omega} = [0, L_1] \times [0, L_2] \times [-h, +h]$ with thickness $2h$ and a rectangular middle plane $\omega = (0, L_1) \times (0, L_2)$. The set ω is partitioned into a mesh of m sub-rectangles, where electrodes or mechanical loads are imposed. We assume a laminated plate consisting of two layers made of two different piezoelectric materials. The parameters z_s and t_s for $s = 1, 2$ (related to the thickness t_s and introduced before in section 3) are defined as

$$z_1 = -\frac{h + h_0}{2} + h_0, \quad t_1 = h + h_0, \quad z_2 = \frac{h - h_0}{2} + h_0, \quad t_2 = h - h_0, \quad (47)$$

where $h_0 \in \mathbb{R}$ is such that $-h < h_0 < h$. Layer 1 is below ω while layer 2 is above, and if $h_0 = 0$ then $t_1 = t_2$ and both layers have the same thickness. If $h_0 > 0$ (respectively, $h_0 < 0$) layer 1 (respectively, layer 2) is thicker than layer 2 (respectively, layer 1).

In the sequel, we fix a 20×20 finite element mesh for the middle plane ω ; the finite elements and the nodes are numbered from the left side $ls = \{0\} \times [0, L_2]$ to the right side $rs = \{L_1\} \times [0, L_2]$ and from the bottom side $bs = [0, L_1] \times \{0\}$ to the top side $ts = [0, L_1] \times \{L_2\}$ of ω . We consider four

types of clamped boundary conditions (abbreviation BC). If $BC = 1$, ω is clamped only on the bottom side ($\gamma_0 = bs$); if $BC = 2$, ω is clamped on the left, bottom and right sides ($\gamma_0 = ls \cup bs \cup rs$); if $BC = 3$, ω is clamped on the two opposite left and right sides ($\gamma_0 = ls \cup rs$); finally, if $BC = 4$, ω is clamped on the two consecutive bottom and right sides ($\gamma_0 = bs \cup rs$). We suppose that the non-zero applied electric potential difference (for actuator multi-objective problem (44)) or the non-zero applied mechanical loads (for the sensor multi-objective problem (46)) may act in $i = 1$ up to $i = 25$ regions consisting of $16 = 4 \times 4$ adjacent finite elements of the 20×20 mesh (we recall that the definition of i is given in (42)), located at the positions $pe \subseteq Y_{16} = \{1, \dots, m_{16} = 25\}$ as explained in Figure 1.

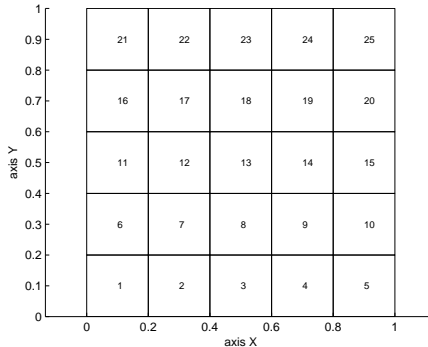


FIGURE 1. Location $pe = [l]$ of each element $l \in Y_{16} = \{1, \dots, 25\}$.

The exact data for the geometry, the electric potential and the mechanical loadings are given in Table 1.

Parameter	Unit	Value	
		(actuator problem)	(sensor problem)
L_1	m	1	1
L_2	m	1	1
h	m	0.01	0.01
φ_0^+	V	-100	0
φ_0^-	V	0	0
$f = (f_i)$	N	(0,0,0)	(10,10,10)
$g = (g_i)$	N	(0,0,0)	(10,10,10)

TABLE 1. Geometric, electric potential and mechanical loadings data.

The piezoelectric, dielectric and elastic coefficients of the two materials (P_{ijk} , ε_{ij} and C_{ijkl}) are given in (48) and Table 2. In particular, the elasticity matrix (C_{ijkl}) in terms of the Young's moduli E_1 , E_2 , E_3 , the Poisson's ratios ν_{12} , ν_{13} , ν_{23} and the shear moduli G_{12} , G_{13} , G_{23} of the material are shown. All the data displayed in Table 2 correspond exactly to two PZT ceramic materials used in [22]. The materials are orthotropic with constant elastic, piezoelectric and dielectric coefficients (cf. Tables VIII and XI in [22]).

$$\begin{bmatrix} P_{111} & P_{122} & P_{133} & P_{123} & P_{131} & P_{112} \\ P_{211} & P_{222} & P_{233} & P_{223} & P_{231} & P_{212} \\ P_{311} & P_{322} & P_{333} & P_{323} & P_{331} & P_{312} \end{bmatrix} = \begin{bmatrix} 0 & 0 & 0 & 0 & P_{15} & 0 \\ 0 & 0 & 0 & 0 & 0 & P_{26} \\ P_{31} & P_{32} & P_{33} & 0 & 0 & 0 \end{bmatrix}$$

$$\begin{bmatrix} \varepsilon_{11} & \varepsilon_{12} & \varepsilon_{13} \\ & \varepsilon_{22} & \varepsilon_{23} \\ sym. & & \varepsilon_{33} \end{bmatrix} = \varepsilon_{33} \begin{bmatrix} 1 & 0 & 0 \\ 0 & 1 & 0 \\ 0 & 0 & 1 \end{bmatrix} \quad (48)$$

$$\begin{bmatrix} C_{1111} & C_{1122} & C_{1133} & C_{1123} & C_{1131} & C_{1112} \\ & C_{2222} & C_{2233} & C_{2223} & C_{2231} & C_{2212} \\ & & C_{3333} & C_{3323} & C_{3331} & C_{3312} \\ & & & C_{2323} & C_{2331} & C_{2312} \\ & sym. & & & C_{3131} & C_{3112} \\ & & & & & C_{1212} \end{bmatrix} = \begin{bmatrix} \frac{1}{E_1} & -\frac{\nu_{12}}{E_2} & -\frac{\nu_{13}}{E_3} & 0 & 0 & 0 \\ & \frac{1}{E_2} & -\frac{\nu_{23}}{E_3} & 0 & 0 & 0 \\ & & \frac{1}{E_3} & 0 & 0 & 0 \\ & & & \frac{1}{G_{23}} & 0 & 0 \\ & & & & \frac{1}{G_{13}} & 0 \\ & & & & & \frac{1}{G_{12}} \end{bmatrix}^{-1}$$

In Tables 1-2 the unit symbols m , V , N , GPa , Cm^{-2} and Fm^{-1} mean, respectively, meter, volt, newton, giga pascal, coulomb per square meter and farad per meter.

6.2. Genetic algorithms. In general, engineering problems involve multiple conflicting objectives. For these problems no single solution that is optimal with respect to all objectives exists. Instead, there is a set of optimal solutions, known as Pareto optimal solutions, reflecting compromises between the objectives. Genetic algorithms (cf. [19]) are population based algorithms and, therefore, particularly suitable to tackle multi-objective problems. They can, in principle, find multiple widely different Pareto-optimal solutions in a single run (cf. [20]). Furthermore, they do not require any differentiability or convexity assumptions and can deal with complex search spaces, as well as non convex Pareto fronts.

Parameter	Unit	PZT-5A Ceramic	PZT-5 Ceramic
		Value	Value
E_1	GPa	67	62
$E_2 = E_3$	GPa	67	54.9
$\nu_{12} = \nu_{13} = \nu_{23}$		0.31	0.31
$G_{12} = G_{13}$	GPa	25.57	23.6
G_{23}	GPa	25.57	18
$P_{31} = P_{32}$	Cm^{-2}	-9.30032142	-12.006
P_{33}	Cm^{-2}	20.3638	17.277
$P_{15} = P_{26}$	Cm^{-2}	14.5749	15.812
ε_{33}	Fm^{-1}	15.31742×10^{-9}	22.99×10^{-9}

TABLE 2. Elastic, piezoelectric and dielectric data of the two materials.

We apply the elitist genetic algorithm, described in [16] to the actuator and sensor multi-objective optimization problems. We note that the genetic algorithm used in this paper is also similar to the one applied in [17] for the analysis of the actuator effect of a single plate made of a transversely isotropic piezoelectric material. However, the mechanical model considered in the present paper is more complex than the one in [17]. In fact, in the present model, the plate is laminated and made of different materials and therefore the tangential and transverse mechanical displacements are coupled (this did not occur in [17]). Moreover we deal with additional optimization variables related to the thicknesses of the layers and the order of the materials. We discuss both the actuator and sensor effects.

We now shortly describe some technical features and the parameters of this genetic algorithm. For both problems (44) and (46), the optimization variables $loc = (i, j, pe)$, t and mat are encoded using binary strings (referred also as chromosomes) with a total length of 30 bits. The first 25 bits represent the sequence of the 25 regions: 1 means that a non-zero electric potential difference or a non-zero mechanical load is applied in this region, while 0 means that the applied electric potential difference or the mechanical load is equal to zero. Since only two materials are considered, the next bit suffices to represent the order of the materials: 1 represents the material vector $mat = (mat_1, mat_2)$, while 0 corresponds to $mat = (mat_2, mat_1)$. The remaining 4 bits of the binary string represent the parameter $h_0 \in \mathbb{R}$ (related to the

thicknesses of the layers, cf. (47)) as a small constant ranging from $-\frac{7h}{8}$ to $\frac{7h}{8}$, allowing 16 values for h_0 .

For the actuator problem, to each string we assign a displacement u , which is the solution of the inner linear system $Ku = F$ in problem (44). For the sensor problem, to each chromosome we assign the vector of the electrical potentials $\varphi|_{\omega^e \times \{z_s\}}$ with $s = 1, 2$, and $e = 1, \dots, m$, where m is the total number of finite elements.

The genetic algorithms is stopped after 100 generations. In all numerical tests we use an initial population size of 100 chromosomes. A tournament selection, a two point crossover and a uniform mutation are adopted. The crossover probability is 0.7. The mutation probability is given by $\frac{1}{b}$, where b is the binary string length, that is $b = 30$. The elitism level considered is 10. The value of sigma share (σ_{share}) is taken equal to 1. For sharing purposes, the distance measure considered is the Hamming distance between chromosomes (cf. [19]).

6.3. Solutions. For all our tests, the stiffness matrices K and force vectors F have been evaluated with the subroutines *planre* and *platre* of the CALFEM toolbox of MATLAB [21]. The genetic algorithms have been implemented in C^{++} .

The Figure 2 shows the objective values d of the Pareto optimal solutions for the actuator multi-objective problem (44) as a function of the number i of regions. We observe an increase of the displacement d with the number of regions i , but for some values of i there are not Pareto optimal solutions. This happens for $23 \leq i \leq 25$ if $BC = 1$, for $22 \leq i \leq 25$ if $BC = 2$, for $20 \leq i \leq 25$ if $BC = 3$, and for $19 \leq i \leq 25$ if $BC = 4$. This means, for example for the latter case $BC = 4$, that to achieve a maximum displacement d it suffices to apply the electric potential difference to 18 regions, because the application of a nonzero electric potential difference in more than 18 regions (in 21 or 23, for example) will not increase the maximum displacement value d .

Analogously, Figure 3 represents the objective values $elpot$ of the Pareto optimal solutions for the sensor multi-objective problem (46) as a function of the number i of regions, where mechanical forces are applied.

We observe the same phenomena as in Figure 2. In general, the objective value $elpot$ increases with the number i , but for some i there are not Pareto

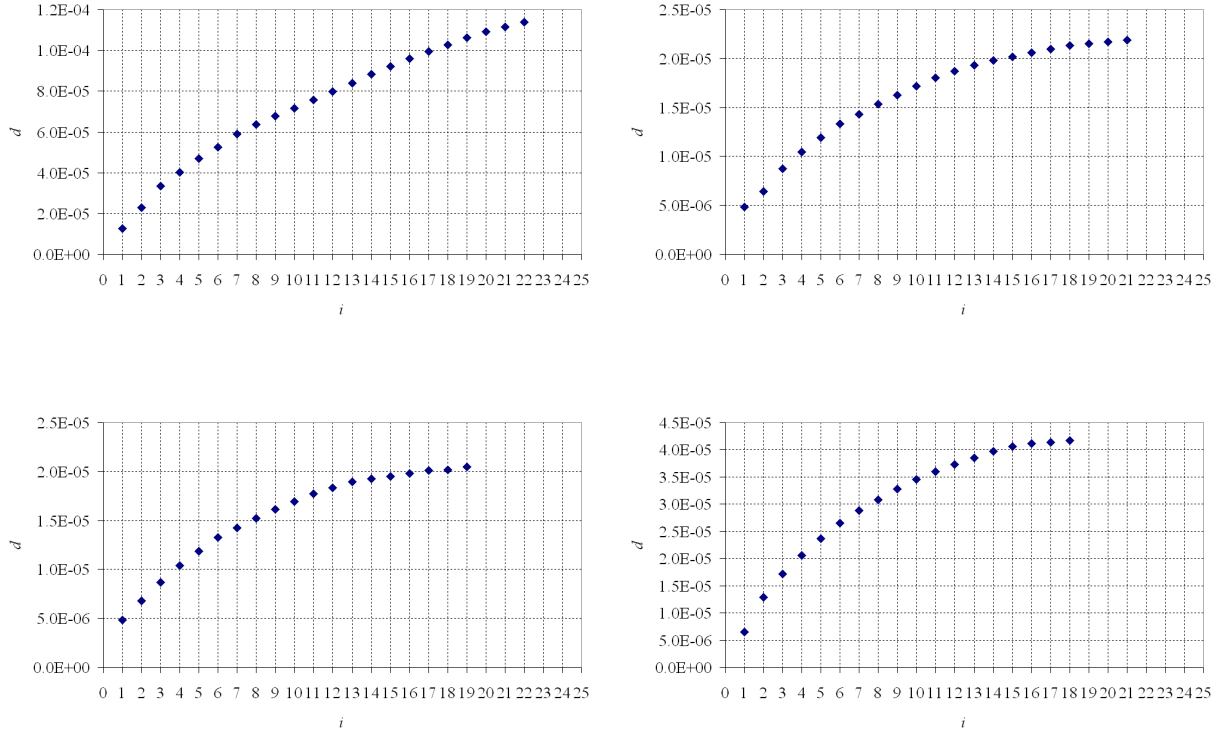


FIGURE 2. Pareto curves: maximal displacement d versus number of regions i (where the electric potential difference $\varphi_0^+ - \varphi_0^-$ is applied) for the actuator multi-objective problem for $BC = 1$ (upper left plot), $BC = 2$ (upper right plot), $BC = 3$ (lower left plot) and $BC = 4$ (lower right plot).

optimal solutions. Namely, for $24 \leq i \leq 25$ if $BC = 1$, for $23 \leq i \leq 25$ if $BC = 2$, for $18 \leq i \leq 25$ if $BC = 3$, and for $22 \leq i \leq 25$ if $BC = 4$.

Some of the Pareto optimal solutions produced by the genetic algorithms are also displayed in Table 3 (for the actuator optimization problem) and Table 4 (for the sensor optimization problem).

In Table 3 *node* represents the number of the node, in which the maximum displacement d is attained. The Figures 4 to 7 (labelling 4 rows in Table 3) represent the plots of the transverse displacements of the plate's middle plane for the corresponding BC , *loc* and *mat*.

In Table 4, e is the number of the finite element where the maximum electric potential $elpot$ is attained for the sensor optimization problem. The Figures 8 to 11 (labelling 4 rows in Table 4) depict the transverse displacement of the plate's middle plane and plot the electric potentials measured at the middle

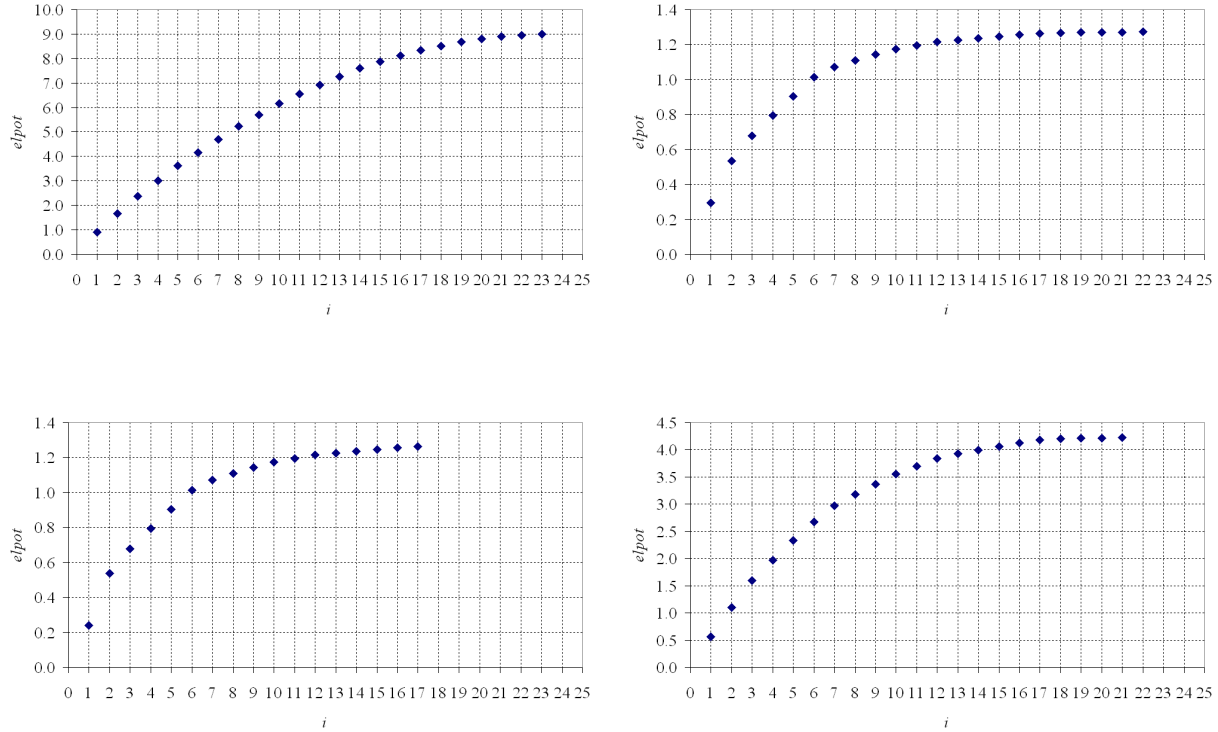


FIGURE 3. Pareto curves: maximal electric potential $elpot$ versus number of regions i (where the mechanical loads are applied) for the sensor multi-objective problem for $BC = 1$ (upper left plot), $BC = 2$ (upper right plot), $BC = 3$ (lower left plot) and $BC = 4$ (lower right plot).

plane of each lamina and at each finite element for the indicated four groups of BC , loc and mat .

In Tables 3 and 4 we have omitted all the symmetric solutions loc , h_0 and mat producing the same objective values d and $elpot$. In fact, due to the symmetry of the plate and the boundary conditions, there are always several locations pe and symmetrical values of h_0 and mat that lead to the same d and $elpot$.

Finally we have also tested the influence of the refinement of the finite element mesh in the numerical results produced by the genetic algorithms. We have done experiments with three meshes with 5×5 , 10×10 and 20×20 finite elements, which means that the variable j in loc becomes $j = 1$ for the 5×5 mesh, $j = 4 = 2 \times 2$ for the 10×10 mesh and $j = 16 = 4 \times 4$ for the 20×20 mesh. For these three different discretizations we observe a similar

BC	$loc = (i, j, pe)$	h_0	$mat = (mat_1, mat_2)$	$node$	d
1 Figure 4 \rightarrow	$(1,4 \times 4, [4])$	0.00125	(PZT-5, PZT-5A)	441	$1.248183E - 05$
	$(2,4 \times 4, [4,5])$	0.00125	(PZT-5, PZT-5A)	441	$2.293397E - 05$
	$(3,4 \times 4, [3,4,5])$	0.00125	(PZT-5, PZT-5A)	441	$3.348424E - 05$
	$(4,4 \times 4, [3,4,5,9])$	0.00125	(PZT-5, PZT-5A)	441	$4.029649E - 05$
	$(5,4 \times 4, [2,3,4,5,9])$	0.00125	(PZT-5, PZT-5A)	441	$4.680007E - 05$
2 Figure 5 \rightarrow	$(1,4 \times 4, [23])$	0	(PZT-5, PZT-5A)	431	$4.818227E - 06$
	$(2,4 \times 4, [17,23])$	0	(PZT-5, PZT-5A)	431	$6.438335E - 06$
	$(3,4 \times 4, [18,23,24])$	0	(PZT-5, PZT-5A)	432	$8.721058E - 06$
	$(4,4 \times 4, [18,19,23,24])$	0	(PZT-5, PZT-5A)	432	$1.042312E - 05$
	$(5,4 \times 4, [17,18,19,22,23])$	0	(PZT-5, PZT-5A)	430	$1.190036E - 05$
3 Figure 6 \rightarrow	$(1,4 \times 4, [3])$	0	(PZT-5, PZT-5A)	11	$4.828368E - 06$
	$(2,4 \times 4, [2,3])$	0	(PZT-5, PZT-5A)	10	$6.808695E - 06$
	$(3,4 \times 4, [2,3,8])$	0	(PZT-5, PZT-5A)	10	$8.708387E - 06$
	$(4,4 \times 4, [2,3,7,8])$	0	(PZT-5, PZT-5A)	10	$1.038399E - 05$
	$(5,4 \times 4, [2,3,7,8,9])$	0	(PZT-5, PZT-5A)	10	$1.183562E - 05$
4 Figure 7 \rightarrow	$(1,4 \times 4, [1])$	0.00125	(PZT-5, PZT-5A)	421	$6.536013E - 06$
	$(2,4 \times 4, [1,2])$	0.00125	(PZT-5, PZT-5A)	421	$1.287488E - 05$
	$(3,4 \times 4, [1,2,3])$	0.00125	(PZT-5, PZT-5A)	421	$1.719750E - 05$
	$(4,4 \times 4, [1,2,3,7])$	0.00125	(PZT-5, PZT-5A)	421	$2.051966E - 05$
	$(5,4 \times 4, [1,2,3,6,7])$	0.00125	(PZT-5, PZT-5A)	421	$2.366497E - 05$

TABLE 3. Solutions loc , h_0 , mat , $node$ and d for the actuator optimization problem (mesh: 20×20).

behavior of the objective values d , $elpot$ and h_0 , mat , as well as a similar location pe for the optimal regions.

7. Conclusion

In this paper, we have developed a piezoelectric model for a thin plate made of a completely anisotropic material. For the sake of validating the model, a laminated plate with two piezoelectric materials of variable thickness is used. For this plate, the actuator and the sensor effects are studied using bi-objective optimizations problems. Due to their characteristics (non-differentiability and non-convexity), genetic algorithms are used to obtain (Pareto-optimal) solutions. For the actuator optimization problem the objectives are to maximize the mechanical displacement while, at the same time, minimize the number of regions where a nonzero electric potential is applied. For the sensor effect, the objectives are the maximization of the electric potential inside the plate while minimizing the number of regions which are subject to mechanical loads. For various boundary conditions we show where

BC	$loc = (i, j, pe)$	h_0	$mat = (mat_1, mat_2)$	e	$elpot$
1 Figure 8 →	$(1, 4 \times 4, [21])$	0.00875	(PZT-5, PZT-5A)	5	0.894998
	$(2, 4 \times 4, [21, 22])$	0.00875	(PZT-5, PZT-5A)	5	1.654821
	$(3, 4 \times 4, [16, 21, 22])$	0.00875	(PZT-5, PZT-5A)	5	2.380768
	$(4, 4 \times 4, [16, 21, 22, 23])$	0.00875	(PZT-5, PZT-5A)	6	3.011719
	$(5, 4 \times 4, [16, 17, 21, 22, 23])$	0.00875	(PZT-5, PZT-5A)	6	3.615470
2 Figure 9 →	$(1, 4 \times 4, [24])$	0.00875	(PZT-5, PZT-5A)	380	0.295855
	$(2, 4 \times 4, [23, 24])$	0.00875	(PZT-5, PZT-5A)	380	0.535390
	$(3, 4 \times 4, [23, 24, 25])$	0.00875	(PZT-5, PZT-5A)	380	0.676532
	$(4, 4 \times 4, [22, 23, 24, 25])$	0.00875	(PZT-5, PZT-5A)	380	0.792569
	$(5, 4 \times 4, [19, 22, 23, 24, 25])$	0.00875	(PZT-5, PZT-5A)	380	0.903534
3 Figure 10 →	$(1, 4 \times 4, [23])$	0.00875	(PZT-5, PZT-5A)	380	0.239884
	$(2, 4 \times 4, [23, 24])$	0.00875	(PZT-5, PZT-5A)	380	0.535988
	$(3, 4 \times 4, [23, 24, 25])$	0.00875	(PZT-5, PZT-5A)	380	0.677186
	$(4, 4 \times 4, [22, 23, 24, 25])$	0.00875	(PZT-5, PZT-5A)	380	0.793471
	$(5, 4 \times 4, [19, 22, 23, 24, 25])$	0.00875	(PZT-5, PZT-5A)	380	0.904455
4 Figure 11 →	$(1, 4 \times 4, [21])$	0.00875	(PZT-5, PZT-5A)	360	0.556523
	$(2, 4 \times 4, [21, 22])$	0.00875	(PZT-5, PZT-5A)	360	1.099163
	$(3, 4 \times 4, [21, 22, 23])$	0.00875	(PZT-5, PZT-5A)	360	1.594584
	$(4, 4 \times 4, [21, 22, 23, 24])$	0.00875	(PZT-5, PZT-5A)	360	1.972989
	$(5, 4 \times 4, [16, 21, 22, 23, 24])$	0.00875	(PZT-5, PZT-5A)	360	2.330120

TABLE 4. Solutions loc , h_0 , mat , e and $elpot$ for the sensor optimization problem (mesh: 20×20).

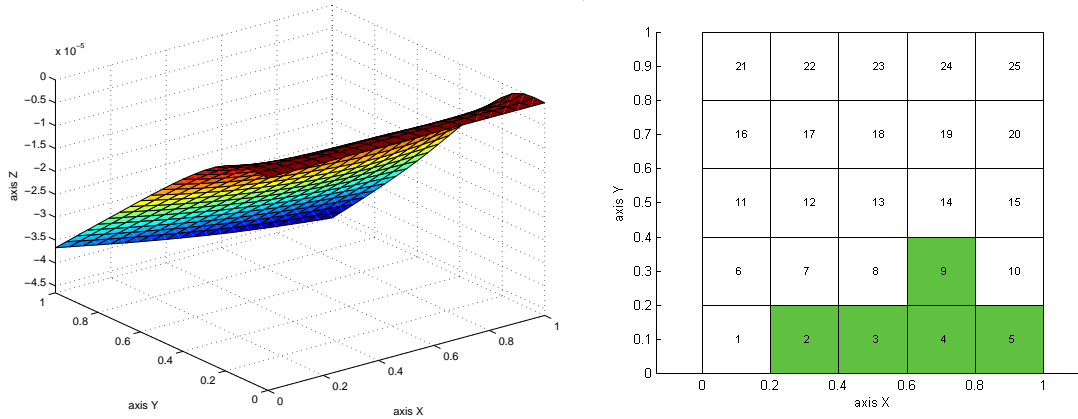


FIGURE 4. Actuator optimization problem: transverse displacement of the plate's middle plane for $BC = 1$ (left plot) and corresponding optimal position $pe = [2, 3, 4, 5, 9]$ of the regions where the non-zero electric potential difference is applied (right plot).

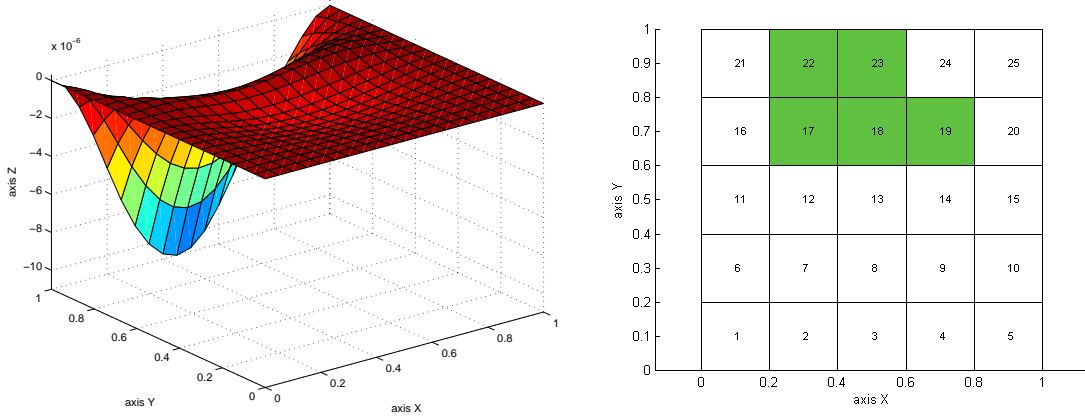


FIGURE 5. Actuator optimization problem: transverse displacement of the plate's middle plane for $BC = 2$ (left plot) and corresponding optimal position $pe=[17,18,19,22,23]$ of the regions where the non-zero electric potential difference is applied (right plot).

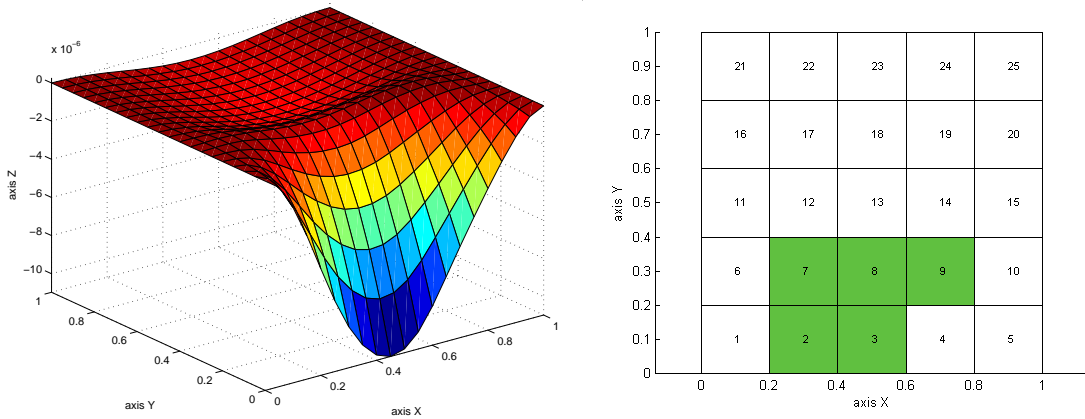


FIGURE 6. Actuator optimization problem: transverse displacement of the plate's middle plane for $BC = 3$ (left plot) and corresponding optimal position $pe=[2,3,7,8,9]$ of the regions where the non-zero electric potential difference is applied (right plot).

to place the applied electric potentials or the mechanical loads, taking into consideration the thickness and the order of the materials. Future work will aim at solving problems with more involved optimization variables and new objectives (e.g., to obtain a predefined mechanical deformation of the plate) using genetic algorithms. Moreover, we also intend to apply techniques from continuous optimization such as optimal control for the investigation and the design of smart materials involving piezoelectric plates.

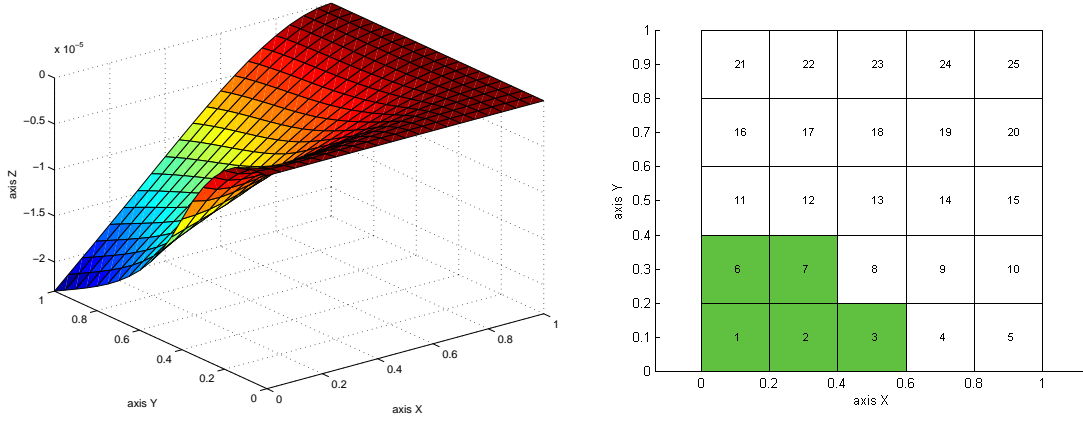


FIGURE 7. Actuator optimization problem: transverse displacement of the plate's middle plane for $BC = 4$ (left plot) and corresponding optimal position $pe=[1,2,3,6,7]$ of the regions where the non-zero electric potential difference is applied (right plot).

Appendix

For the general case of anisotropy the modified coefficients $A_{\alpha\beta\gamma\rho}$, $p_{3\alpha\beta}$ and p_{33} appearing in equation (8) are defined by

$$A_{\alpha\beta\gamma\rho} = C_{\alpha\beta\gamma\rho} - \frac{C_{\alpha\beta 33}C_{33\gamma\rho}}{C_{3333}} + C_{\alpha\beta 33} \frac{C_{\nu 333}}{C_{3333}} b_{\delta\nu} a_{\delta\gamma\rho} - C_{\alpha\beta\nu 3} b_{\delta\nu} a_{\delta\gamma\rho},$$

$$p_{3\alpha\beta} = P_{3\alpha\beta} - \frac{C_{\alpha\beta 33}}{C_{3333}} P_{333} + C_{\alpha\beta 33} \frac{C_{33\nu 3}}{C_{3333}} b_{\delta\nu} c_{\delta} - C_{\alpha\beta\nu 3} b_{\delta\nu} c_{\delta},$$

$$p_{33} = \varepsilon_{33} + \frac{P_{333}P_{333}}{C_{3333}} - P_{333} \frac{C_{33\nu 3}}{C_{3333}} b_{\delta\nu} c_{\delta} + P_{3\nu 3} b_{\delta\nu} c_{\delta},$$

where

$$a_{\delta\gamma\rho} = C_{33\gamma\rho}C_{\delta 333} - C_{\delta 3\gamma\rho}C_{3333}, \quad c_{\delta} = C_{\delta 333}P_{333} - C_{3333}P_{3\delta 3},$$

$$[b_{\delta\nu}] = [C_{\delta 333}C_{33\nu 3} - C_{\delta 3\nu 3}C_{3333}]^{-1} \quad (\text{identity between two matrices}).$$

References

- [1] T. Ikeda, *Fundamentals of Piezoelectricity*, Oxford University Press, New York, 1990.
- [2] R. Smith, *Smart material systems: model development*. (Frontiers in applied mathematics ; 32) Philadelphia: SIAM, 2005.

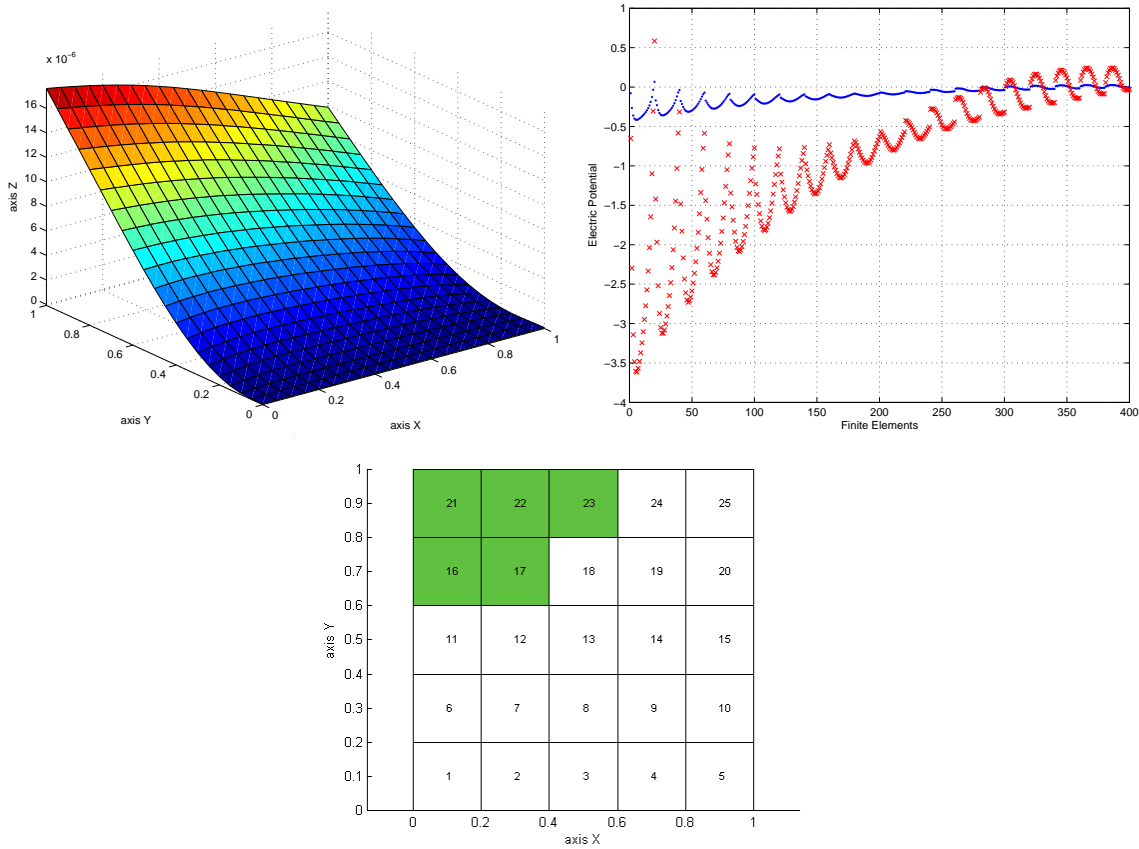


FIGURE 8. Sensor optimization problem: transverse displacement of the plate's middle plane for $BC = 1$ (upper left plot), electric potentials (cross mark - $\varphi|_{\omega^e \times \{z_1\}}$ on lamina 1 and dotted - $\varphi|_{\omega^e \times \{z_2\}}$ on lamina 2) (upper right plot) and corresponding optimal position $pe = [16, 17, 21, 22, 23]$ of the regions where the non-zero mechanical forces are applied (lower plot).

- [3] P.G. Ciarlet, *Mathematical Elasticity, Volume II: Theory of Plates*, North-Holland, Amsterdam, 1997.
- [4] G.A. Maugin and D. Attou, An asymptotic theory of thin piezoelectric plates, *Quarterly Journal of Mechanics & Applied Mathematics* **43**, 347-362, 1990.
- [5] M. Rahmoune, A. Benjeddou and R. Ohayon, New thin piezoelectric plate models. *Journal of Intelligent Material Systems and Structures*, **9**, 1017-1029, 1998.
- [6] A. Sene, Modelling of piezoelectric static thin plates, *Asymptotic Analysis*, vol. 25 (1), pp. 1-20, 2001.
- [7] A. Raoult and A. Sene, Modelling of piezoelectric plates including magnetic effects, *Asymptotic Analysis*, vol.34 (1) pp. 1-40, 2003.
- [8] I. N. Figueiredo and C. F. Leal, A piezoelectric anisotropic plate model, *Asymptotic Analysis*, **44**, 3-4, 327-346, 2005.

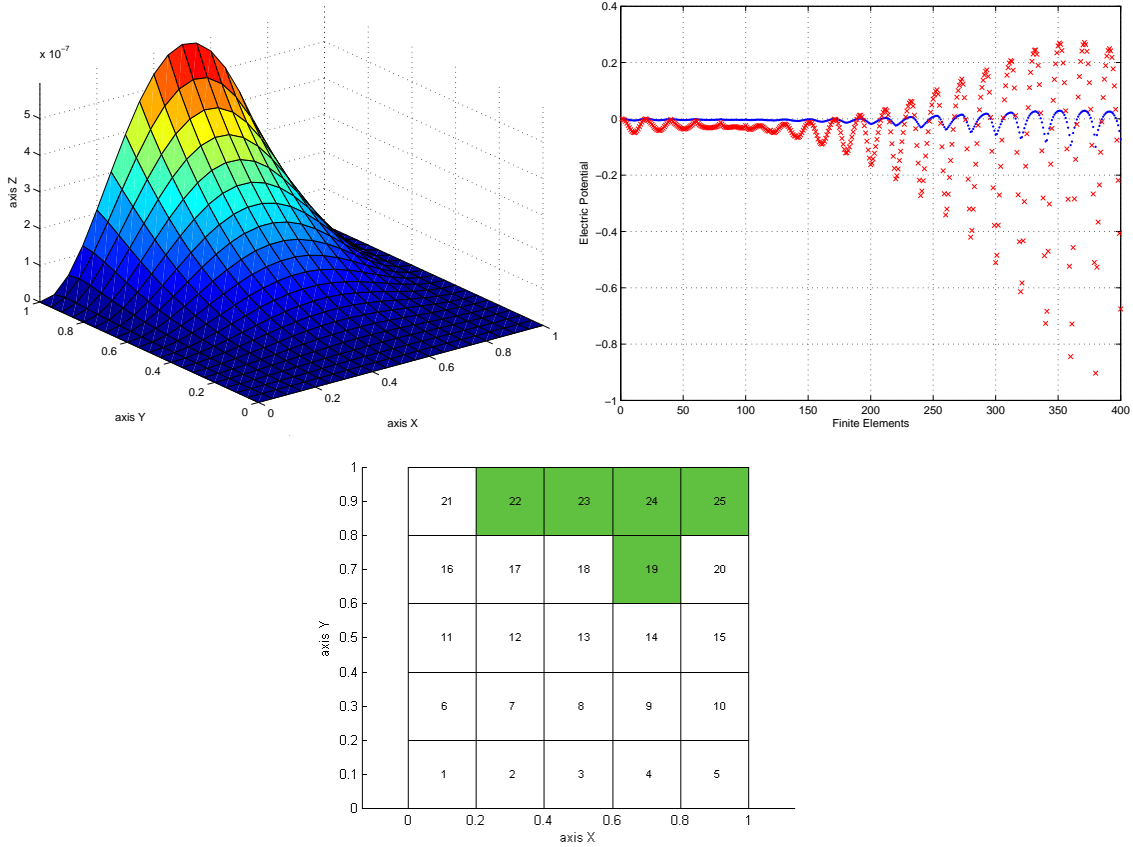


FIGURE 9. Sensor optimization problem: transverse displacement of the plate's middle plane for $BC = 2$ (upper left plot), electric potentials (cross mark - $\varphi|_{\omega^e \times \{z_1\}}$ on lamina 1 and dotted - $\varphi|_{\omega^e \times \{z_2\}}$ on lamina 2) (upper right plot), and corresponding optimal position $pe = [19, 22, 23, 24, 25]$ of the regions where the non-zero mechanical forces are applied (lower plot).

- [9] C. Collard and B. Miara, *Two-dimensional models for geometrically nonlinear thin piezoelectric shells*, *Asymptotic Analysis*, **31**, 2 113-151, 2003.
- [10] M. Bernadou and C. Haenel, *Modelization and numerical approximation of piezoelectric thin shells. I. The continuous problems*, *Computer Methods in Applied Mechanics and Engineering*, **192**, 37-38 4003-4030, 2003.
- [11] M. Bernadou and C. Haenel, *Modelization and numerical approximation of piezoelectric thin shells. II. Approximation by finite element methods and numerical experiments*, *Computer Methods in Applied Mechanics and Engineering*, **192**, 37-38 4045-4073, 2003.
- [12] M. Bernadou and C. Haenel, *Modelization and numerical approximation of piezoelectric thin shells. III. From the patches to the active structures*, *Computer Methods in Applied Mechanics and Engineering*, **192**, 37-38 4075-4107, 2003.

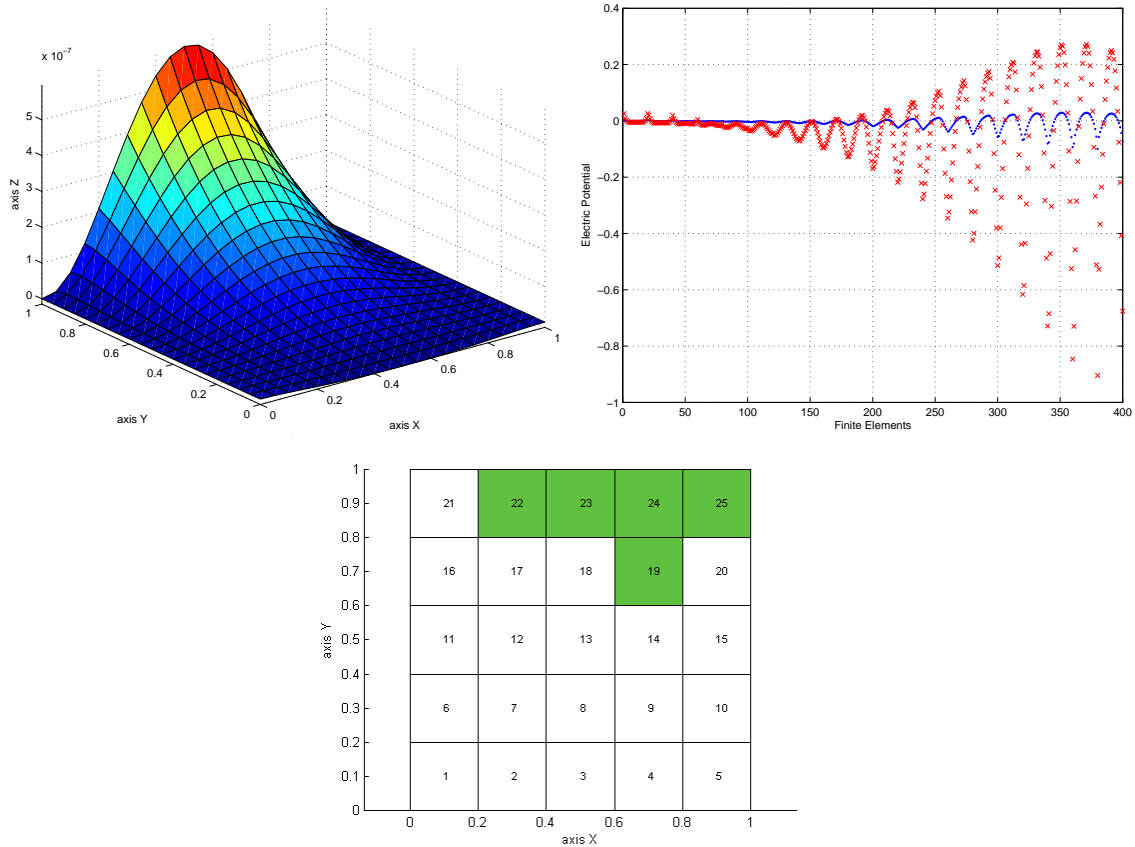


FIGURE 10. Sensor optimization problem: transverse displacement of the plate's middle plane for $BC = 3$ (upper left plot), electric potentials (cross mark - $\varphi|_{\omega^e \times \{z_1\}}$ on lamina 1, and, dotted - $\varphi|_{\omega^e \times \{z_2\}}$ on lamina 2) (upper right plot) and corresponding optimal position $pe = [19, 22, 23, 24, 25]$ of the regions where the non-zero mechanical forces are applied (lower plot).

- [13] W. Geis, A.-M. Sändig and G. Mishuris, Piezoelectricity in Multi-layer Actuators: Modelling and Analysis in Two and Three-Dimensions, *Preprint IANS, 2003/23, Univ. Stuttgart, Germany*, 2003.
- [14] W. Geis, G. Mishuris and A.-M. Sändig, Asymptotic models for piezoelectric stack actuators with thin metal inclusions, *Preprint IANS, 2004/01, Univ. Stuttgart, Germany*, 2004.
- [15] W. Geis, Numerical simulation of linear models for piezoelectric stack actuators, *Preprint IANS, 2005/07, Univ. Stuttgart, Germany*, 2005.
- [16] L. Costa and P. Oliveira, An elitist genetic algorithm for multiobjective optimization, in M.G.C. Resende and J.P. de Sousa (eds.), *Metaheuristics: Computer Decision-Making*, pp. 217-236, Kluwer Academic Publishers, 2003.
- [17] L. Costa, P. Oliveira, I.N. Figueiredo and R. Leal, Actuator effect of a piezoelectric anisotropic plate model. *Mechanics of Advanced Materials & Structures* (to appear 2006) (also Preprint

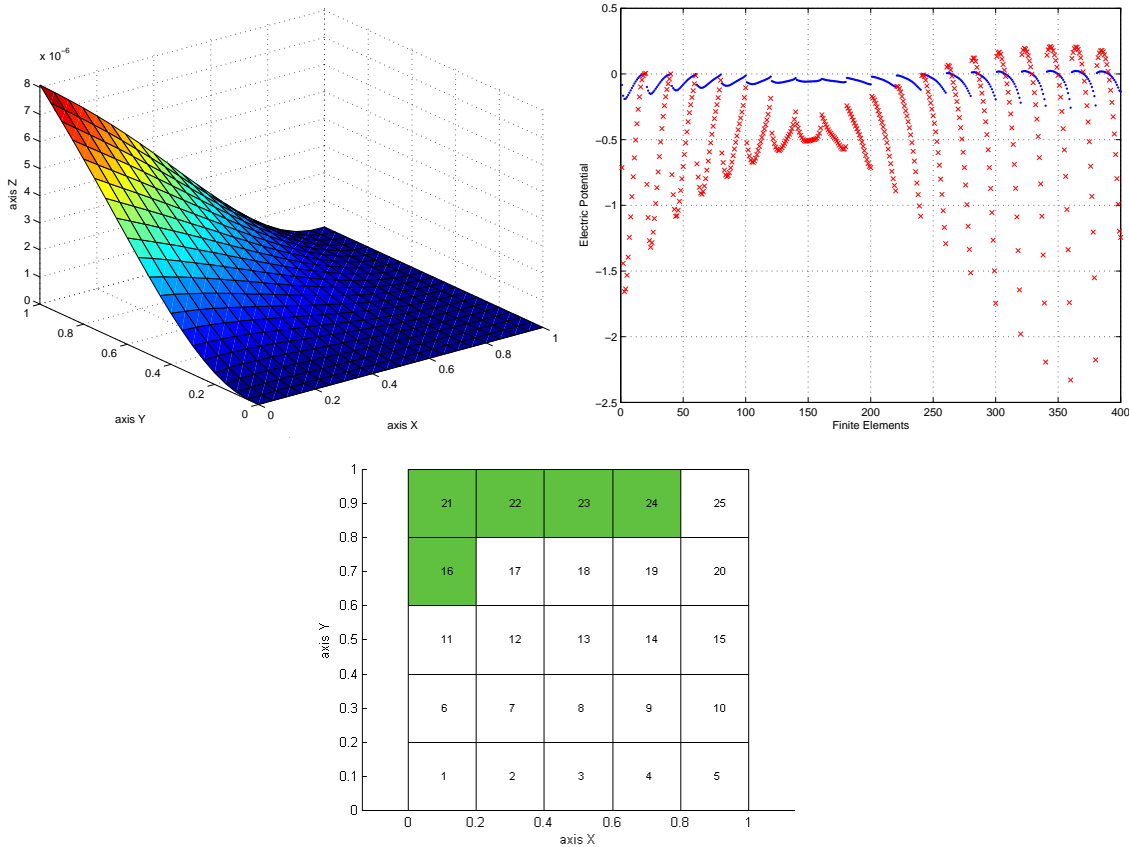


FIGURE 11. Sensor optimization problem: transverse displacement of the plate's middle plane for $BC = 4$ (upper left plot), electric potentials (cross mark - $\varphi|_{\omega^e \times \{z_1\}}$ on lamina 1, and, dotted - $\varphi|_{\omega^e \times \{z_2\}}$ on lamina 2) (upper right plot) and corresponding optimal position $pe = [16, 21, 22, 23, 24]$ of the regions where the non-zero mechanical forces are applied (lower plot).

05-06 Department of Mathematics, University of Coimbra, Portugal, and available from <http://www.mat.uc.pt/~isabel/publica.html>.

- [18] P.G. Ciarlet, *The Finite Element Method for Elliptic Problems*, North-Holland, Amsterdam, 1978.
- [19] D. Goldberg, *Genetic Algorithms in Search, Optimization, and Machine Learning*. Reading, Mass. Addison-Wesley, 1989.
- [20] K. Deb, *Multi-Objective Optimization using Evolutionary Algorithms*, John Wiley & Sons, England, 2001.
- [21] CALFEM (<http://www.byggmek.lth.se/CALFEM>), *A finite element toolbox to MATLAB, Version 3.4*, Structural Mechanics and Solid Mechanics, Department of Mechanics and Materials, Lund University, Sweden, 2004.

- [22] S. Klinkel and W. Wagner, A geometrically nonlinear piezoelectric solid shell element based on a mixed multi-field variational formulation. *International Journal for Numerical Methods in Engineering*, **65**, 3, 349-382, 2006.

L. COSTA

DEPARTAMENTO DE PRODUÇÃO E SISTEMAS, ESCOLA DE ENGENHARIA, UNIVERSIDADE DO MINHO, CAMPUS DE AZURÉM, 4800-058 GUIMARÃES, PORTUGAL

E-mail address: lac@dps.uminho.pt

URL: <http://sarmiento.eng.uminho.pt/dps/lac/>

I. FIGUEIREDO

DEPARTAMENTO DE MATEMÁTICA, UNIVERSIDADE DE COIMBRA, APARTADO 3008, 3001-454 COIMBRA, PORTUGAL

E-mail address: isabelf@mat.uc.pt

URL: <http://www.mat.uc.pt/~isabelf/>

R. LEAL

DEPARTAMENTO DE ENGENHARIA MECÂNICA, UNIVERSIDADE DE COIMBRA, PINHAL DE MARROCOS, 3001-201 COIMBRA, PORTUGAL

E-mail address: rogerio.leal@dem.uc.pt

P. OLIVEIRA

DEPARTAMENTO DE PRODUÇÃO E SISTEMAS, ESCOLA DE ENGENHARIA, UNIVERSIDADE DO MINHO, CAMPUS DE AZURÉM, 4800-058 GUIMARÃES, PORTUGAL

E-mail address: pno@dps.uminho.pt

URL: <http://sarmiento.eng.uminho.pt/dps/pno/>

G. STADLER

DEPARTAMENTO DE MATEMÁTICA, UNIVERSIDADE DE COIMBRA, APARTADO 3008, 3001-454 COIMBRA, PORTUGAL

E-mail address: georgst@mat.uc.pt

URL: <http://www.mat.uc.pt/~georgst/>